

SURFACE MODIFICATION OF THERMOPLASTIC POLYMERS FOR LATERAL
FLOW ASSAY APPLICATIONS

by

Md Shamim Mahmud, B.S.

A thesis submitted to the Graduate Council of
Texas State University in partial fulfillment
of the requirement for the degree of
Master of Science
with a Major in Engineering
August 2018

Committee Members:

Namwon Kim, Chair

Bahram Asiabanpour

Ravi Droopad

COPYRIGHT

by

Md Shamim Mahmud

2018

FAIR USE AND AUTHOR'S PERMISSION STATEMENT

Fair Use

This work is protected by the Copyright Laws of the United States (Public Law 94-553, section 107). Consistent with fair use as defined in the Copyright Laws, brief quotations from this material are allowed with proper acknowledgement. Use of this material for financial gain without the author's express written permission is not allowed.

Duplication Permission

As the copyright holder of this work I, Md Shamim Mahmud, authorize duplication of this work, in whole or in part, for educational or scholarly purposes only.

DEDICATION

I dedicate my work to my parents, for always supporting and helping me pursue my dreams.

ACKNOWLEDGEMENTS

First and foremost, I would like to express my sincere gratitude to my advisor, Dr. Namwon Kim. It has been my great honor to be his M.Sc. student. I appreciate his many years of patient guidance, inspiration and support to stimulate my M.Sc. experience. I would also like to extend my gratitude to the members of my committee, Dr. Bahram Asiabanpour, Dr. Ravi Droopad, who provided encouraging and constructive feedback. I am grateful for their helpful comments and suggestions on all stages of this project.

TABLE OF CONTENTS

	Page
ACKNOWLEDGEMENTS	v
LIST OF TABLES	viii
LIST OF FIGURES	ix
NOMENCLATURE	xii
ABSTRACT	xiv
CHAPTER	
1. INTRODUCTION	1
1.1 Motivation	1
1.2 LFA device	2
1.3 Objective	3
1.3.1 Capillary driven microfluidics	4
1.3.2 Fabrication	4
1.3.3 Detection methods	4
1.3.3.1 Chemiluminescence detection	4
1.3.3.2 Gold nanoparticle detection	5
2. LITERATURE REVIEW: MICROFLUIDIC DEVICES FABRICATED WITH THERMOPLASTIC POLYMER	6
2.1 Introduction	6
2.2 PMMA materials	7
2.3 Laser technology	8
2.4 Surface Activation	10
3. DEVELOPMENT OF LASER ABLATED POLYMER MICROCHANNELS	13
3.1 Introduction	13
3.2 Instrument setup	15
3.3 Laser parameter optimization:	17
3.4 Laser micromachining	20

3.5 Chemical treatment	23
4. SURFACE AND CAPILLARY FLOW CHARACTERIZATION	25
4.1 Roughness	26
4.2 Surface Chemistry Analysis:.....	29
4.3 Contact angle.....	30
4.4 Capillary flow rate	33
4.4.1 Water.....	34
4.4.2 Glycerol	36
5. THEORETICAL AND EXPERIMENTAL ANALYSIS.....	40
5.1 Physics of capillary flow.....	40
5.2 Theoretical model selection	41
5.2.1 Predicted model 1, for flow dynamics calculation	41
5.2.2 Predicted model 2, for flow dynamics calculation	47
5.2.3 Predicted model 3, for flow dynamics calculation	48
5.3 Theoretical and experimental result comparison:	51
6. ASSAY PREPARATION.....	55
6.1 Device fabrication	58
6.1.1 Reservoirs	58
6.1.2 Channel formation	58
6.1.3 Test line formation.....	58
6.1.4 Wicking reservoir	59
6.2 Solution preparation	59
6.3 Protein immobilization and characterization	60
7. CONCLUSION	62
APPENDIX SECTION.....	64
REFERENCES	83

LIST OF TABLES

Table	Page
1. Different laser pulse energy and laser fluence	18
2. Different components and their liquid properties	36

LIST OF FIGURES

Figure	Page
1. Compact lateral flow device, assembly with several parts	2
2. a) Pulse duration b) Pulse repetition rate	9
3. Schematic for UV-curable super-hydrophilic polyacrylate coating film chemically grafted on a glass substrate	11
4. Zwitterionic Polymer grafting.....	12
5. Laser mirror setup.....	15
6. Aperture controlling.....	16
7. X-Y stage controlling.....	16
8. Microcontroller box and Visual basic program, PPP= Pulse per point, Xp (Number of points in X direction), Yp (Number of points in the Y direction), Xs (Number of steps in the X direction), Ys (Number of steps in the Y direction)	17
9. Dependence of the ablated area on PMMA surface by the number of accumulated laser pulses at the fluence of $\Phi= 2.96 \text{ J/cm}^2$	19
10. Contact angle after 1 hour of laser ablation and roughness vs. laser pulse number	20
11. 444 μm width of the channel	21
12. 671 μm width of the channel	22
13. Parallel channel creation.....	22
14. Laser setup and surface modification	22
15. Hydrocarbon position in AOT chain.....	24
16. Rounded micro-grooved formation in an air medium	27

17. a) Multichannel, b) Single channel	27
18. Profilometer image.....	28
19. Isometric View.....	28
20. Surface morphology by different laser pulse steps of 65 μm , 80 μm , 110 μm , and 125 μm in the y- direction.....	29
21. Oxygen free radicals	30
22. a) Before laser treatment; b) Right after laser treatment.....	31
23. Hydrophobic recovery after 1 hour of laser Ablation.....	32
24. a) Surfactant treated b) Without surfactant.....	33
25. Physical setup: High-speed camera	34
26. Capillary Driven flow	35
27. Progress of the liquid meniscus, with time, t, corresponding to the different channel width. (RMS = 0.99).....	35
28. a) 20% glycerol-water b) 40% glycerol-water c) 60% glycerol-water d) DOI water e) surfactant-water solution surface tension measurement	37
29. Different viscous liquid with a channel width of ($W = 444 \pm 5 \mu\text{m}$).....	37
30. Laser pulse overlap, dx (x directional laser movement), dy (y directional laser movement), the blue color shows the ablated area and the red color represents the 83% overlap of that blue color area.	38
31. In a fixed width ($W = 444 \pm 55 \mu\text{m}$), with the change of laser pulse steps capillary flow can be controlled, and follow the governing equation (RMS=0.99)	39
32. Capillary force creation due to surface tension.....	40
33. Capillary driven flow and its behavior through the equation	42

34. Microgroove dimensions for the analytical formula of roughness factor, r	43
35. Capillary flow and surface tension inside the channel.....	43
36. Flow separation and merge in the multiple channels.....	49
37. Theoretical and experimental comparison of the dynamic coefficient (k) in no-slip boundary condition	51
38. Meniscus shape changes during the capillary flow.....	53
39. Cross section of the microchannel (80 μm depth)	54
40. Multiscale rough surface fabrication via laser irradiation and corresponding capillary driven flow	54
41. Solid works modeling PMMA device.....	57
42. Multiple laser ablation and pillar creation	59
43. a) Without antigen and antibody reaction b) Color change with the presence of antibody and antigen	61
44. Left: Compact PMMA device, Middle: Nitrocellulose device, Right: PMMA device the possible replacement of Nitrocellulose membrane only	61

NOMENCLATURE

γ_{s-g}	Solid gas interfacial tension (N/m)
γ_{l-s}	Liquid solid interfacial tension(N/m)
θ	Contact angle (Degrees)
C_s	Critical micelle concentration (m/l)
Γ_s	Gibbs adsorption coefficient
θ_E	Pristine PMMA contact angle (Degrees)
r	Surface roughness parameter
k	Dynamic coefficient (mm ² /s)
σ	Surface tension (N/m)
Δp	Pressure difference (N/m ²)
μ	Dynamic viscosity (mPa-s)
t	Time (s)
Bo	Bond number
ρ	Density (kg/m ³)
R	Reynolds number
G	Gravity (N/kg)
We	Weber number
x	Distance travel by liquid (mm)
p	Aspect ration
$g(p)$	Geometric shape factor

Q..... Volumetric flow rate (m³/s)

ABSTRACT

Lateral flow immunoassay (LFIA) is the technology behind low-cost, simple, rapid and portable detection devices which is popular in biomedicine, agriculture, food and environmental sciences. In this research, a simple and inexpensive manufacturing procedure has been introduced to develop lateral flow assay device. Laser micromachining was applied on the thermoplastic poly (methyl methacrylate) (PMMA) polymer to change the surface topography, and the surfactant solution added to the following laser treated surface to achieve the capillary driven flow. A nanosecond pulsed excimer laser was used to ablate a rectangular area of 4 mm × 40 mm on a precleaned PMMA substrate under an ambient condition to introduce capillary driven flow on the PMMA substrate and to change the surface chemistry. It was found that the density of the functional groups (-C-O-, -O-H) created by the laser irradiation and capillary flow rates depend on the laser scanning steps, surface roughness and laser fluence. Since the surface recover from hydrophilic to hydrophobic following the laser treatment, the ionic surfactant AOT (dioctyl sulfosuccinate sodium salt) with 0.08 M was applied to the surface to introduce more polar group on the surface. The surfactant solution reduces the liquid-solid interfacial tension, and therefore induces capillary driven flow. A speed of capillary driven flow up to 16 mm/s can be achieved on the laser and surfactant treated surface when the step sizes of scanning the laser beam in the x-y directions were 50 μm and 500 μm, respectively. However, no capillary driven flows were observed when the step size of scanning laser beam were 250 μm and 250 μm or 500 μm and 500 μm in the

x - y directions respectively. Therefore, the capillary flow rate on the treated surface could be controlled by changing the laser scanning steps which helped to create more microgrooves on the surface. The proposed method of combining laser and surfactant treatment is suitable for cost-effective manufacturing of long-lasting thermoplastic polymer-based lateral flow strips. Finally, the performance of the laser modified PMMA strip had been successfully tested by introducing antibody and antigen reaction on the fabricated device. The overall result entails the better prospect of the PMMA device as a possible replacement of nitrocellulose membrane.

1. INTRODUCTION

1.1 Motivation

In the past century, lateral flow assay has played a vital role in the medical industry. Lateral flow assay is a device which is used to detect the antigen and antibody reaction on the top of the polymer surface. The Chinese invented the first iteration of this device and primarily used it for saliva-based diagnostics [1]. The primary technical based lateral flow assay was developed in 1956 by Plotz and Singer [2]. Early development of the lateral flow assay device was used for human pregnancy test, which gradually shifted to the food industry, urine and blood testing for medical diagnostic purpose. This device includes the technology as nitrocellulose membrane manufacturing, antibody generation, fluid dispensing and processing equipment as well as different methodologies of the manufacturing system. All these elements are required to transform the complex system into the simple system to provide prognostic results in a variety of critical applications. The first compact products of lateral flow were commercially introduced to the market in the late 1980s. Since then, the technology has gradually evolved, and manufacturing in this industry has also seen an increase. There are 200 companies worldwide producing lateral flow assay device and doing business on over \$2.1 billions of dollars (USD). The application also expanded well beyond the clinical diagnostics area to agriculture, biowarfare, food, environmental health, and safety. So, there is still some area where we can improve this technology, like nitrocellulose membrane replacement with polymer, antigen and antibody binding on the polymer surface, etc. The primary purpose of this research is to introduce low-cost fabrication techniques and characterize the surface property in the form of a fluid mechanics perspective to produce highly efficient lateral flow assay device.

1.2 LFA device

Lateral flow assay (LFA) which is also known as lateral flow immune Assay (LFIA) consists of four individual parts, which are: sample pad, conjugate pad, nitrocellulose membrane, and reservoir (Fig.1). In the whole system, a nitrocellulose membrane is the most important part, where the capillary driven flow takes place. Based on this flow speed, antigen and antibody reaction takes place on the test line. Future advancements that can be foreseen in this field would be studies on the replacement of the nitrocellulose membrane with any other material that can show similar features to the original membrane. In the sample pad, the antigen sample is dropped, and it accumulates with the nanoparticle in the conjugate pad. Then, the antigen passes through the nitrocellulose membrane and reacts with the antibody which already inhabits in the test line. The chemical reaction emits a signal by changing the color; the rest of the fluid doesn't react with antibody reserve in a wick chamber.

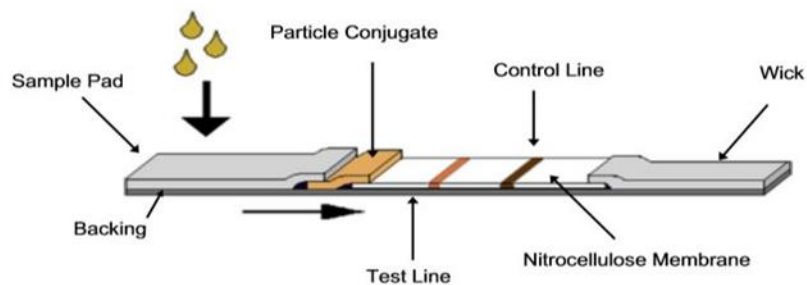


Fig. 1. Compact lateral flow device, assembly with several parts [3]

1.3 Objective

Rapid detection technology with high sensitivity and selectivity of antibody and antigen detection are required in a diagnostic test. Traditional laboratory benchtop techniques are time-consuming and require complex sample handling. LFIA systems offers a detection alternative, where all detection steps are on one portable miniaturized device. The overall objective of this work is to introduce a new fabrication technique to replace the contemporary nitrocellulose membrane which is used as a reaction matrix in present LFIA devices. The generic example of this application of such a model is the design of minimally invasive biomedical diagnostic tools in which a small amount of liquid sample enters a capillary channel and dissolves the bio-molecules, which reacts with the chemically active product already inhabited on the surface and detect the chemical reaction.

To achieve the objectives, the following steps have been taken:

- The appropriate material selection which can replace the nitrocellulose membrane.
- Manufacturing methodology selection to fabricate porous surface.
- Characterize the capillary driven flow inside the microchannel.
- Protein binding on the surface: finding the surface treatment technique that can easily attach the antibody to the selected material.
- Compare the capillary dynamics with an analytical model of an extended version of the Lucas-Washburn equation.

1.3.1 Capillary driven microfluidics

The capillary driven microfluidic device has been introduced in this thesis, where, the development of this surface driven method will have a significant impact on the point of care diagnostic (POC). Compared to traditional microfluidic devices, which rely on external force to introduce flow inside the channel, our capillary driven LFIA's are self-driven which depend on surface energy and the surface wetting properties. Therefore, no external power is needed for the pumping. In this thesis, polymer substrate is used to introduce capillary driven flow into the microchannel. The reasoning for this choice will be discussed in Chapter 3.

1.3.2 Fabrication

There are several methods which are currently used in fabricating the surface. In this research, laser micromachining has been used to modify the surface property. The cost is minimized by using poly (methyl methacrylate) (PMMA) and poly (carbonate) (PC) as a substrate which can be applied for a roll to roll continuous process for large-scale manufacturing.

1.3.3 Detection methods

1.3.3.1 Chemiluminescence detection

First, it has been chosen to detect the chemical reaction using chemiluminescence (CL) because it is an attractive option for detection in which analytic binding causes photochemical emission. When compared to fluorescence, no excitation source is needed. Therefore, no specific radiation is required. However, CL does not allow to observe the chemical reaction in the presence of light. That is the limitation of CL detection. That encourages choosing the 2nd method of gold nanoparticle detection.

1.3.3.2 Gold nanoparticle detection

The list of materials used in LFIAs is very vast which includes gold nanoparticles. Gold nanoparticles is one of the most commonly used pieces of equipment in point of care diagnostics (POC). This nanoparticle has a very high affinity for biomolecules and can readily be functionalized. The optical property of gold nanoparticles depends on their size and shape [4]. It also has a high affinity for the proteins which is one of its unique features. LFA device sensitivity depends on gold nanoparticles' optical properties [5]. Gold nanoparticles absorb and scatter the light due to their strong interaction with light. The conduction of electrons undergoes a collective oscillation when they are excited by light in visual wavelengths. The oscillation is known as a surface plasmon resonance (SPR). This optical property of gold nanoparticles is highly dependent on the nanoparticle diameter. Smaller nanoparticles absorb the light and have a peak near 520 nm, while the larger nanoparticles absorb more longer wavelengths.

2. LITERATURE REVIEW: MICROFLUIDIC DEVICES FABRICATED WITH THERMOPLASTIC POLYMER

2.1 Introduction

The microfluidic-based lab on a chip or biosensor offers several advantages. A biosensor is an analytical device which sends the signal in the measurable limit to detect the existence of desired biological component. The signal change can be measured electronically using a transducer. Moreover, a microfluidic device contains micro/nonporous channel to allow fluid transportation. The microfluidic device can be divided into five systems depending on the driving source they use: capillary driven, pressure driven, centrifugal, electro kinetics and acoustic system. In this research, the capillary driven microfluidic device is developed for lateral flow applications. There are an abundance of benefits to use a capillary driven miniaturized microfluidic device such as less sample consumption, fewer cost per analysis, high sensitivity, and maneuverability. Since materials for substrates play a vital role in fabricating useful microfluidic devices, so the performance of the microfluidic device is defined by material selection. Protein immobilization and fluid handling all are related to substrate property. The device can be fabricated on silicon or glass material [6]. The idea has been brought from the semiconductor industry, where photolithography, wet etching, dry etching and plasma etching are used to the fabricate microchannels. Silicon is not optically transparent, and is difficult for micromachining, so glass is the available option. Though the glass is optically transparent, not flexible. The polymer could be a good choice, and it has bright future for flexible device fabrication [7]. FDM (fused deposition modelling) prototyping is the current method to fabricate the microfluidic device using flexible

polymeric material [8]. Besides that, injection molding [9], optical lithography [10], laser ablation [11] and X-ray lithography [12] are also used. Recently paper-based inexpensive microfluidic device have been fabricated, but the limitation of this device [13] is due to protein adhesion.

2.2 PMMA materials

It has been discussed that polymer could be the best available choice for the next generation of microfluidic device development. Poly (methyl methacrylate) PMMA is also commercially known as Plexiglas, whose contact angle is relatively less than 90° , meaning it is hydrophilic. The glass transition temperature of the PMMA substrate is between 105° - 130° °C. It is mechanically stable, but the primary problem is its susceptibility to becoming solvent. Although the primary focus is on PMMA substrate, it also relevant to other material such as polycarbonate (PC). Though a variety of methods are used to form a microfluidic channel, one of the important rapid prototyping processes is hot embossing. In this process, the temperature raises in glass transition temperature and finally applies a master mold structure on the PMMA substrate in specific force to create desired fabric on the top of the PMMA surface [14]. Hot embossing is also used to fabricate closed microchannels. On the other hand, the laser is the contemporary fabrication method that can produce microchannels efficiently and can deploy for the rapid prototyping. Also, laser microfabrication is good to fabricate open microchannels. This research is primarily focusing on open microchannel device fabrication.

2.3 Laser technology

The laser is a concentrated light which has different energy level based on its pulse regime. There are three types of pulse regime in the laser system: nanosecond, picosecond, and femtosecond. The intense laser light produced higher thermal energy and that energy used for material processing [15]. More recently the laser processing is used for machining the metallic material [16]. The ability of the laser is to precisely machine micron and sub-micron features and the ranges of laser pulse duration between nanosecond to picosecond which demonstrates the significant morphological difference in laser processed material. In this case, selecting the appropriate laser system is one of the critical factors in laser micromachining. Laser systems are also used in the formation of ligand-free collodion nanoparticles [17]. In nanosecond laser ablation, ablated time on the target material is much longer than any other laser system. In this case, a longer pulse duration helps to generate high heat which is longer than the thermalization time of most metals where 10-100 ps are the standard range of copper and stainless-steel micromachining [18]. However, there is little evidence of laser micromachining application in the material processing industry regarding precision and controllable ablation. In a section of the thesis, we are going to discuss the laser parameters that are related to the energy emitted by the laser system. Two types of parameters are used in laser processing that are pulse duration and pulse repetition rate, where, the pulse duration is described as FWHM (full-width half of the maximum) amplitude of the laser pulse. On the other hand, pulse repetition rate is defined as the number of the pulses emitted per second. Fig. 2 describes the laser parameters [19].

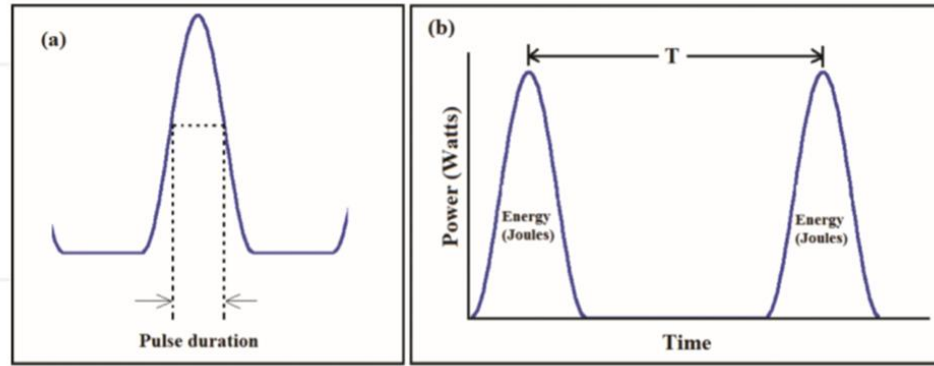


Fig. 2. a) Pulse duration b) Pulse repetition rate [19]

In this research, the nanosecond pulse laser system is used due to the availability of resources and for the longer ablation duration. Because of longer pulse duration, the laser gets enough time to interact with the material. It irradiates the materials and leads to continuous heating of the substrate. The laser pulse energy will then be spread outside of the heating zone by the conduction process and causes the irradiated target to boil and evaporation. This boiling and evaporation of the target material leads to the production of an uncontrollable melt layer [20]. It is apparently assumable that the laser pulse duration affects the target material. Now, the question is how far the impact could be? This question will be answered step-by-step in the following sections. Before going to a depth of the experimental analysis, we are going to describe the theoretical modeling.

Longer pulse duration increases the threshold fluence and decreases the effective energy penetration depth. The main effect is that vaporization of the target substrate requires much more energy than melting. Usually, electron and lattice temperature will remain at the same thermal equilibrium point if the laser pulse duration is long in comparison with the electron-phonon energy transfer time.

The laser fluence equation would be [19]:

$$f \sim \rho \Omega D^{1/2} \times \tau_L^{1/2}$$

D is the heat diffusion coefficient, Ω the specific heat of evaporation, τ energy-transfer time. ρ material density.

2.4 Surface Activation

Surface properties play an important role when capillary driven flow takes place on the polymer surface. Making a microporous surface on the top of polymer surface does not necessarily mean that the capillary driven flow will take place. In this case, hydrophilicity is one of the primary criteria to transport the liquid. Recently experimentation has been done to improve surface hydrophilicity [21]. Also, the functionalized surface is essential for the immobilization of biomolecules to develop POC device [22]. The PMMA surface can be activated variously. Plasma etching, UV, Atom Transfer Radical Polymerization (ATRP) and as well as several chemical reaction processes.

Plasma contains electrons and ions which strongly interact with the polymer surface. As a result, physical and chemical changes take place. It is an effective surface modification method for biomaterials. It has been found that the plasma surface modification takes place hundred angstroms to 10 mm depth into the bulk material [23] and greatly increases the hydrophilicity. The existence of the higher amount of hydroxyl and peroxy groups could be the possible reason for hydrophilicity. The surface roughness has also increased with the plasma etching duration. There are different types of gaseous materials are used for plasma etching such as O₂, N₂, Ar and NH₃ in various pressure and time condition.

Among them, N_2 and NH_3 is powerful because it incorporate both nitrogen and oxygen-containing groups where O_2 and Ar incorporate only with oxygen containing group [24]. Besides that, when PMMA is exposed to UV ray, methyl ester groups result in a functional carboxyl group [25]. If the surface is treated in UV rays in an Ozone environment after the initial exposer, the contact angle significantly reduces rather than UV exposer in ambient condition. Not only UV ray directly used to create a functional group on the surface, but also it used as a catalyst of a chemical reaction. Too.L mentioned that UV curable super-hydrophilic polyacrylate coating could be possible to develop [26]. In that paper, polyacrylate coating film had been chemically grafted on the surface of c-methacryloxy propyl trimethoxy silane modified glass substrate via UV exposer (Fig. 3).

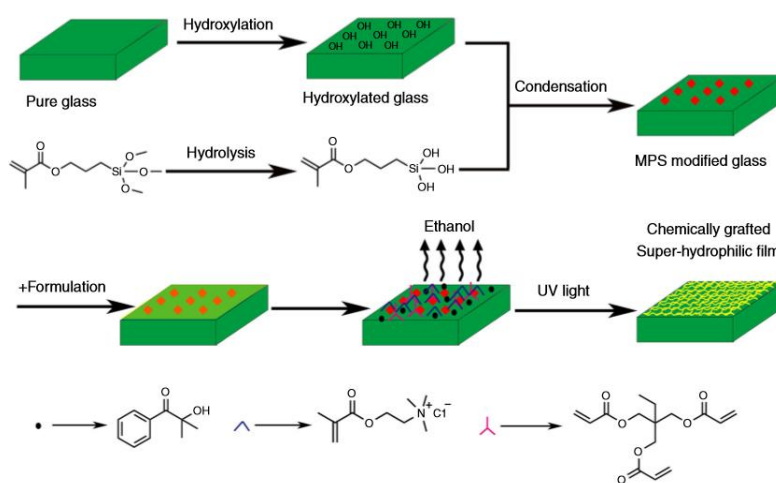


Fig. 3. Schematic for UV-curable super-hydrophilic polyacrylate coating film chemically grafted on a glass substrate [26]

Coating a surface with biomolecules is another way for the functionalization of polymer surface, which is capable of absorbing the liquid. Atom transfer of radical polymerization (ATRP) is one where the atom transfer is the crucial step in the reaction responsible for

uniform polymer chain growth. One of the examples is carbon nanotube that is functionalized and grafting synthesis of styrene-acrylonitrile (SAN) using ATRP process [27]. In the above process, sophisticated reaction chamber is required to functionalize the surface as well as time-consuming. There is, however, another way to avoid ATRP process and functionalize the surface to introduce Zwitterionic Polymer on the surface. In zwitterionic polymer, there are two polar groups, positive and negative, both are actively working on the surface (Fig. 4). However, this process also goes through multiple reaction steps [28]. In this case, the laser is one of the most significant choices, which could activate the surface as well as change the surface structure.

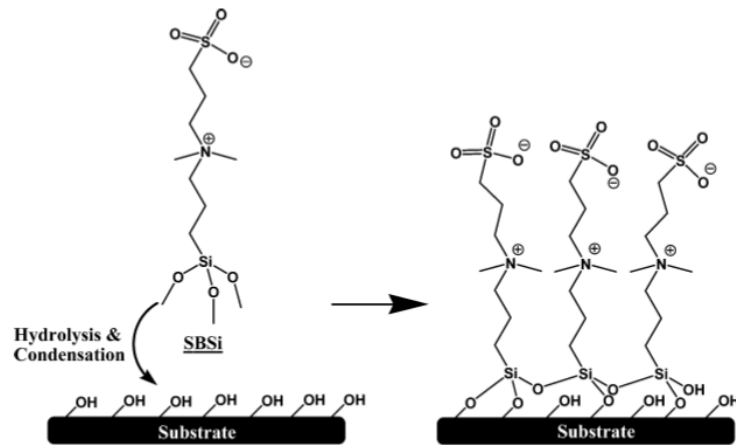


Fig. 4. Zwitterionic Polymer grafting [28]

PMMA is well suited for low-cost microfluidic device fabrication. Laser microfabrication is one example of rapid prototyping micro/nanofabrication techniques that help to reduce the fabrication cost. The surface of PMMA can be easily modified using the chemical and physical methods, and it is also possible to immobilize the biomolecules on PMMA substrate. In conclusion, low cost and rapid fabrication are both important parameters used to develop PMMA microfluidic devices in mass scale production.

3. DEVELOPMENT OF LASER ABLATED POLYMER MICROCHANNELS

3.1 Introduction

Before going to discuss the microchannel formation, we need to know why and how microchannel helps to transport the liquid. The formation of microchannels do not necessarily mean it will carry the fluid. If the surface properties of the channel are not favorable, flow can be severely inhibited or even prevented. Microchannels only carry the fluid when the surface of the microchannel is superhydrophilic. The term superhydrophilic comes from the name hydrophilicity. Hydrophilicity means liquid absorbed by the surface. So, the liquid and surface contact angle would be less than 90° . In the case of superhydrophilicity, the surface and liquid contact angle must be less than 5° . In this research, the superhydrophilic property has been tested to be added into the microchannel surface.

Superhydrophilicity is not an old term, and the research on making superhydrophilic surface has been started since the late 1990s. There are several techniques which are used to make surface superhydrophilic. Molecular deposition and surface chemistry modification can achieve the enhancement of hydrophilicity of the surface [29]. Molecular deposition over the inorganic substrate is common whereas surface chemistry modification procedure is used in the polymer material. Theoretically, any natural or synthetic material could be converted to the superhydrophilic surface by applying the chemical treatment and mechanical roughening of the surface. After introducing of nanotechnology, the inorganic nanomaterials, such as: titanium oxide (TiO_2) [30], zinc oxide (ZnO) [31], silica (SiO_2) [32] are common materials to introduce superhydrophilicity on the surface. These nanoparticles are deposited on the substrate

from either solution, ink-jet printing, sol-gel technique, spin coating or through a sputtering process. Poor stability is one of the main reasons for avoiding the physically deposited film. The polymer is also suitable for use as a coated material, but their surface is not too hydrophilic. Also, it needs more surface modification by introducing oxidation process. Polyvinyl alcohol (PVA) is a polymer used extensively in the plastics industry in molding compounds, surface coating, and chemical resistant films. A mixture of PVA and hydroxypropyl methylcellulose (HPMC) can be spin coated on the surface to create a stable low contact angle on the substrate. In this case, the contact angle reduced to 20° but the goal of reaching a contact angle less than 5° was not achieved.

Superhydrophilicity can be achieved in two ways, either increasing the surface energy of the substrate or reducing the surface tension of the liquid. Surface roughness and chemical changes increase surface energy. In the previous chapter, we discussed the plasma etching and UV irradiation. Both etches the surface and changes the surface chemistry. The wavelength of photons carry heaps of energy, and break the intermolecular bond of most polymer, provoking structural and chemical changes of the macromolecules. The UV and plasma irradiation also causes crosslinking and increases the density of oxygen based polar groups in the surface region [33]. However, both strategies lack surface roughness. We have come to know that superhydrophilic surface cannot be achieved without satisfying roughness parameters of the surface [34]. UV and plasma only create few nanometers of surface roughness that don't fulfill the roughness parameters. Though it temporarily creates superhydrophilicity, it does not last long, because hydrophobic recovery takes place. The relation between surface roughness and superhydrophilicity as well as hydrophobic recovery will be discussed in chapter 4. Now

to overcome this problem a laser has been used due to the laser's high thermal energy which helps to physical and chemical changes of the polymer.

3.2 Instrument setup

A nanosecond pulsed excimer laser (COMpexPRO 201, Coherent Inc., Santa Clara, CA) is used for this experiment. The wavelength, pulse repetition rate, and fluency of the laser were 248 nm, 10 Hz, and 2.96 J/cm², respectively. A unique setup is built to control the laser and drive it in the desired direction. A mirror is set up within an inclination angle 45°, which transfer the laser ray horizontal to the vertical direction (Fig. 5).

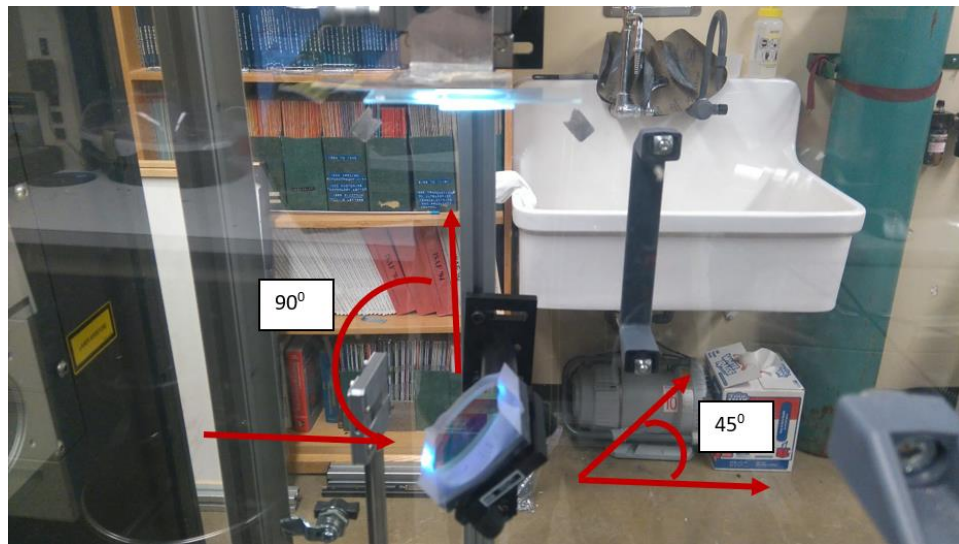


Fig. 5. Laser mirror setup.

The reflected laser will pass through the aperture, which is setup with millimeter gauge knob which contains a rectangular shaped passage. By controlling the knob, formation of different size of a rectangular shaped aperture is possible as shown in Fig. 6.

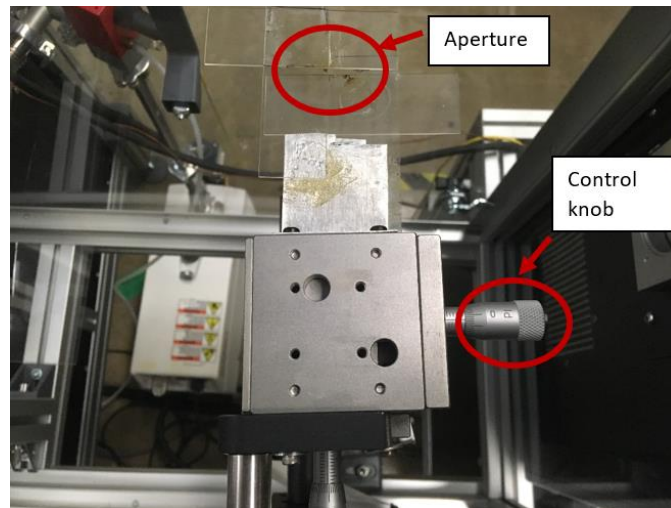


Fig. 6. Aperture controlling

There is a lens above the aperture which helps to concentrate the light on the sample. An automated X-Y stage controller is setup above the lens where the sample usually put. It mainly controls the movement of the sample in X and Y direction with synchronizing the laser pulse. All those setups are constructed based on mathematical calculation of laser parameters and x-y stage movements where the laser light concentration would be high enough to ablate the target material (Fig. 7).

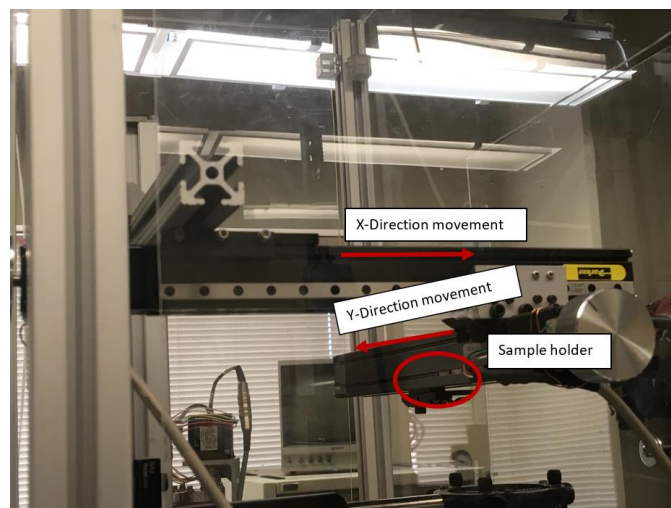


Fig. 7. X-Y stage controlling

The microcontroller box controls the X and Y stage and the programming has been done in visual basic in Atmel studio, which synchronizes the laser pulse number with stage movement. We can control the laser pulse number and X-Y movement parameters manually through the input parameter in the program. Instead of changing the program in every setup, an external switch has been developed in microcontroller box to input the settings manually (Fig. 8). The input value changes the program setup automatically, and the pulse generated according to those inputs.

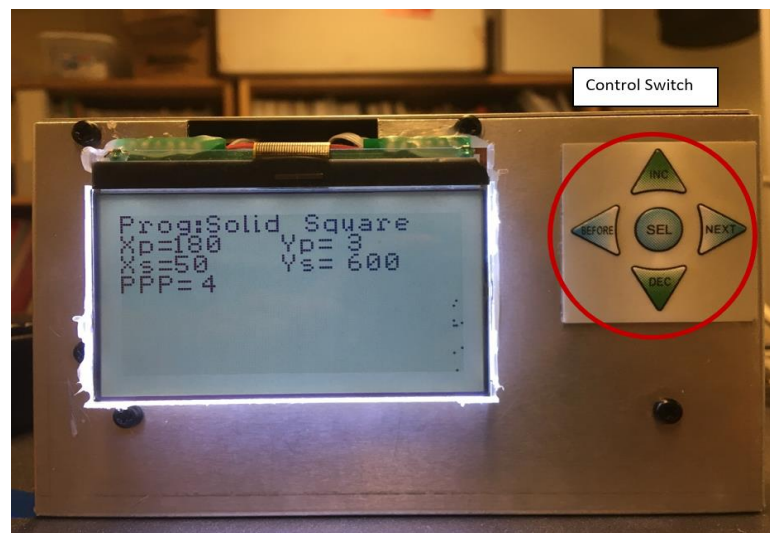


Fig. 8. Microcontroller box and Visual basic program, PPP= Pulse per point, Xp (Number of points in X direction), Yp (Number of points in the Y direction), Xs (Number of steps in the X direction), Ys (Number of steps in the Y direction)

3.3 Laser parameter optimization

The system provides energy in the range of 200 mJ- 600 mJ depending upon the availability of gas sources. Here in this research, 300mj energy is used in (NGR) mode with a frequency of 10Hz. Laser fluence is the energy which is count as the energy passes through the square shape aperture area. The energy is calculated using the energy

measurement device and the calculated energy is divided by the aperture area. Here the laser fluence in different energy mood is:

Table 1: Different laser pulse energy and laser fluence	
Laser Pulse Energy (mJ)	Laser Fluence (J/cm ²)
200	2.24
250	2.468
300	2.96
350	3.12
400	3.4

The selected laser fluence was 2.96 J/cm². If we use the high laser fluence for the continuous long run machining purpose, laser fluence could be disrupted. Because when we use 2 or 3 hours of continuous laser machining, the fluence fluctuate due to lack of oxygen supply. The optimum oxygen supply can be found in the lower energy level around 200 mj-300 mj. For the uniform machining purpose lower laser fluence and high pulse number are used, because laser pulse number and laser fluence is vice versa. The amount of energy emits by the lower pulse number, and upper fluence is equal to the higher pulse number and lower fluence.

In order to determine the number of laser pulse, laser ablation has been done on plane PMMA substrate by observing the ablated area. With the increase of laser pulse number, the ablated area is increased. At a certain point where the laser pulse number N~189, the ablated area turns to a saturated condition. This means the increase of laser pulse number only helps to penetrate the substrate, but not to increase the ablated area (Fig. 9).

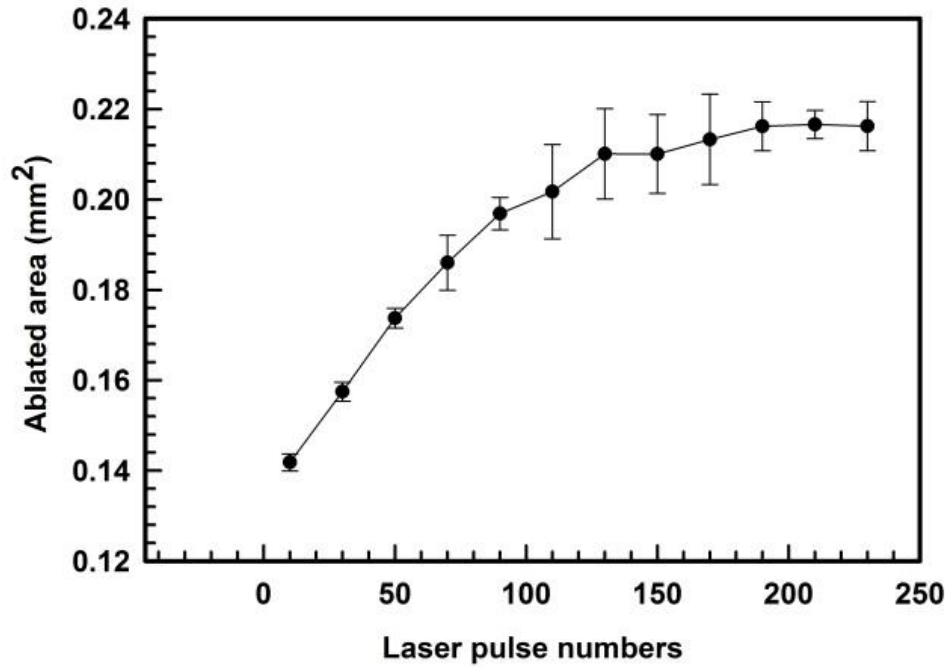


Fig. 9. Dependence of the ablated area on PMMA surface by the number of accumulated laser pulses at the fluence of $\Phi = 2.96 \text{ J/cm}^2$

Higher pulse number creates more thermal ablation, and it forms deeper microgrooves and more porous structures causing the surface to roughen, where the contact angle reduces with the increase of surface roughness. The relation between surface roughness and the contact angle is a mathematically derived formula which will be discussed in section IV. However, we need lower contact angle to introduce capillary driven flow inside the microchannel. As a result, we need higher laser pulse number. The PMMA substrate is used in this research is too thin estimated between 0.03 inch or 762 μm so it did not allow to go higher laser ablation which will ablate the surface and creates a hole in the substrate. Overcoming this problem, a plot has been done between surface roughness, contact angle and laser pulse number as shown in Fig. 10. The figure represents that with the increase of laser pulse number, contact angle decreases and

surface roughness increases. When we use the laser pulse number 3 and 4 we found the lower capillary speed but higher transparent surface; as well as, laser pulse number 7,8,9 we found higher capillary speed in lower transparency. As we need to maintain high transparency to fabricate the device so, the rest of the part of this research laser pulse number 5 has been used for the experiment. It also relates to the substrate thickness that the depth of cut doesn't overcome the material thickness.

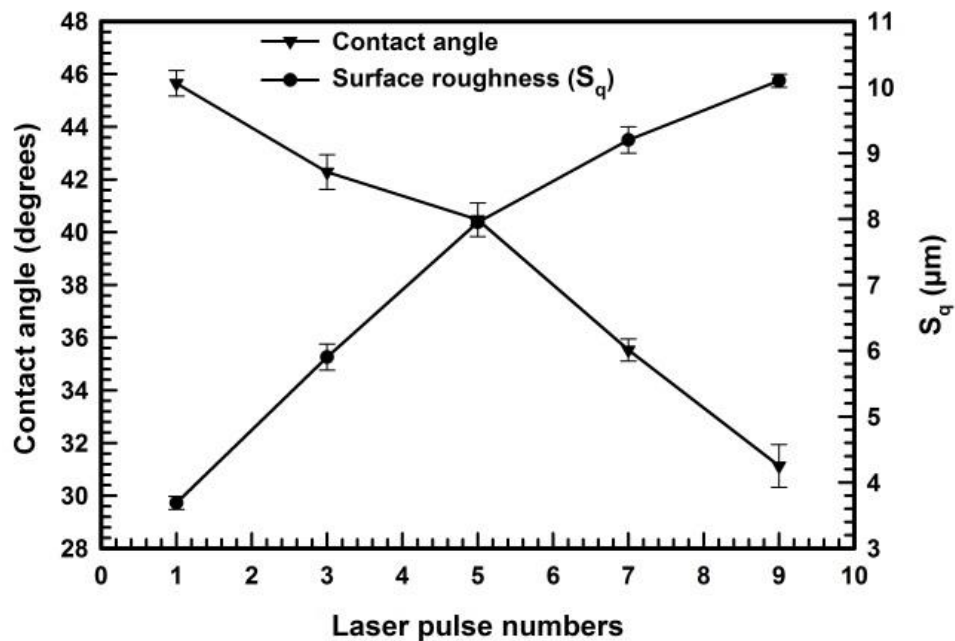


Fig. 10. Contact angle after 1 hour of laser ablation and roughness vs. laser pulse number.

3.4 Laser micromachining

Clear PMMA sheets (0.03 in thick Plexiglas®, ePlastics, San Diego, CA) were cut into 60 mm × 40 mm rectangular substrate. To ensure a clean surface, the PMMA substrate was cleaned in ethanol and rinsed with 10 min sonication in DI water. Before

the laser ablation, the substrates were stored in a convection oven at 40 °C for 30 min to remove water molecules. Preliminarily the aperture size was set up 300 μm \times 300 μm and gradually changed to 300 μm \times 700 μm to form different size of microchannels.

In the **1st experiment**, the PMMA substrate was put on the sample holder of the X-Y stage. In this case, the aperture size was 300 μm \times 450 μm where Y was 300 μm , and X was 450 μm . According to the program, the laser moved in the Y direction every 50 μm and the laser pulse number was 5 for each movement. It indicates in the Y direction at 300 μm space; the laser ray overlaps 83% and $5 \times 6 = 30$ (5 the pulse number and 6 the number of steps in 300 μm distance) times energy gain by the substrate. For creating a 40 mm long channel, an 800 pulse point is needed. To reach every point laser need to move 50 μm ; $800 \times 50 = 40000$ μm or 40 mm. The width of the laser was 450 μm . So, the width of the ablated microchannel 444 μm (Fig. 11).

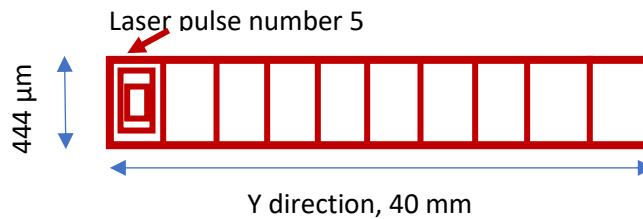


Fig. 11. 444 μm width of the channel

Subsequently the aperture width was changed from 300 μm to 700 μm and different width of the channel was fabricated to observe the capillary driven flow inside the channel (Fig. 12).

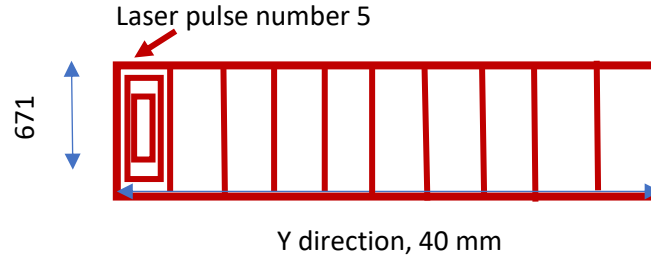


Fig. 12. 671 μm width of the channel

In the **2nd experiment**, aperture size was 300 μm × 450 μm and the laser pulse step was changed X and Y both direction where Y direction was 50 μm, and X-direction was 500 μm by fixing the laser pulse number 5, same as before (Fig. 13).

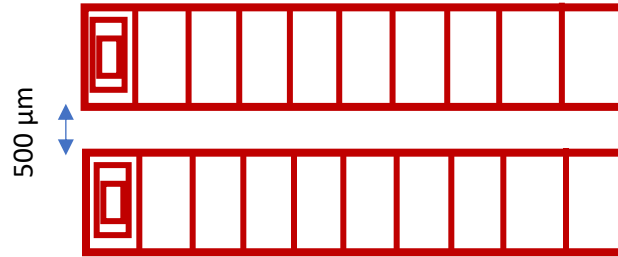


Fig. 13. Parallel channel creation

The whole system and laser processing steps.

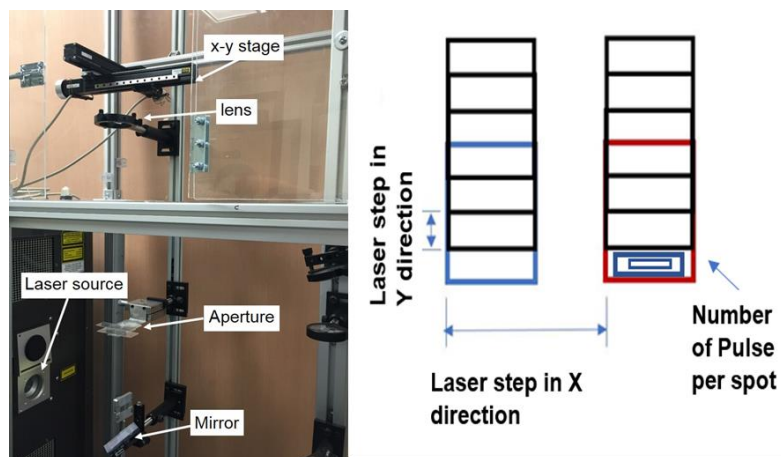


Fig. 14. Laser setup and surface modification

3.5 Chemical treatment

The surfactant is a molecule which attracts the polar group of the liquid. Using surfactant on laser treated surface will introduce more function group on the surface. Different types of surfactant have been analyzed before selecting the desired surfactant. There are two types of surfactant available in the market: Ionic and nonionic. The ionic surfactant has a polar group in the chain molecule, so it is useful when absorbing the liquid. In this research, dioctyl sulfosuccinate sodium salt (97% AOT, Sigma-Aldrich, St. Louis, MO) was used as a surfactant. The surfactant was mixed with DI water at the volume ratio of 1:29. The concentration of the surfactant solution was 0.08M. If we increase the concentration of surfactant solution, it will absorb the more liquid due to the existence of the polar group. However, it is found at the concentration level 0.08M the surfactant solution reached the critical micelle concentration (CMC) level where the increase of concentration does not affect the absorption rate. Wetting phenomena of a water droplet on substrates are of crucial concern in our daily life. The wetting behavior depends on two factors, the chemical composition and the roughness of the solid surface. AOT surfactant solution helps to satisfy the young equation [35]

$\cos\theta = (\gamma_{s-g} - \gamma_{l-s})/\gamma_{l-g}$ by reducing the liquid-solid interfacial tension less than solid-gas interfacial tension $\gamma_{l-s} < \gamma_{s-g}$ [36] here γ_{l-s} is the tension force between liquid and solid; γ_{s-g} is tension force between solid and gas. Surfactant molecules tend to be absorbed by the l-g and l-s interface and therefore change the surface property and wetting behavior of the surface. Gibbs adsorption equation describes the absorption of surfactant onto the interface. $\Gamma_s = -(1/K_B T)(d\gamma/d \ln c_s)$, where C_s is greater than critical micelle concentration; Γ_s , K_B and T is absorption coefficient, Boltzmann constant and temperature

subsequently. AOT is an ionic surfactant, which has two identical hydrocarbon tails (Fig. 15). The wetting behavior depends with the branches of the surfactant chain. As AOT has the hydrocarbon branches, it helps to attract the polar group of water molecules.

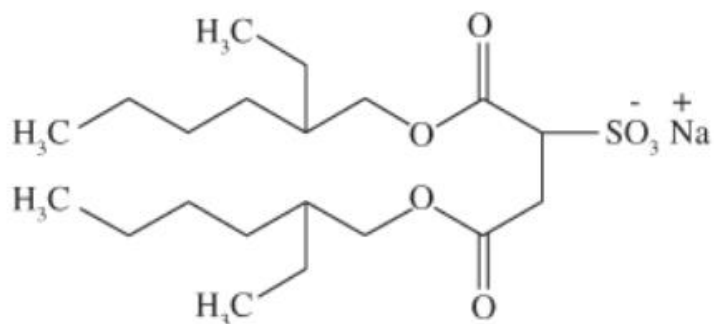


Fig. 15. Hydrocarbon position in AOT chain, Ref: Sigma Aldrich

The double-tailed surfactant is thermodynamically stable because it reduces the interfacial-free energy associated with microlevel water contacts and it also experiences stronger volume interaction [37]. After each laser ablation, the PMMA substrate was stored at room temperature more than 5 hours and then merely rinsing the substrate into the surfactant solution. After the 5 min of surfactant treatment, the substrate was dried at 40 °C in a temperature-controlled convection oven for 30 min.

4. SURFACE AND CAPILLARY FLOW CHARACTERIZATION

It is observed that wetting properties of specific natural surfaces are a direct consequence of hierarchical micro and nanostructures existing on a surface [38]. Creating micro-structures by ultrafast lasers [39] in specific ambient environments is useful, because it produces multi-scale surface roughness [40] via a simple one-step process, without the need of a clean room facility or high vacuum equipment requirements. Also, a variety of materials can be used as a substrate for laser ablation [41]. There are two primary purposes of laser ablation: topographical changes introducing desired surface texture and microstructural changes which alter the crystalline structure. Different types of laser create different types of structures on the surface. Femtosecond lasers create dominant growth spike, whereas the nanosecond laser are ablation dominant. In ablation dominant laser system, spikes remain below the original surface. On the other hand, in growth dominant, spikes grow top of the original substrate. The medium where the laser ablation takes place has a significant influence on the spike morphology [42]. It is found in a different medium such as SF₆, Cl₂, N₂ and air different surface structures are formed [43]. It is also observed that laser treatment in SF₆ or Cl₂ mediums creates a highly fine conical structure where SF₆ generates a more significant amount of surface roughness in compared to the Cl₂-prepared structures. Air or N₂ medium treated surface showed more rounded morphology than those made in halogen-containing gasses. The structured form in different gas medium also depends on the density of the gas. The high density of gas helps to produce more structure. Surfaces which were laser treated in SF₆ yielded the highest density of the conical structure, followed by those treated in Cl₂ medium. The laser works as thermal ablation machine when the laser heated the surface, the energy

interacts with the substrate and removed material by vaporization. In such processes, micro and nano-sized features are created on the surface, which increases surface roughness. The spike of the rough surface and the microstructure formed by the laser ablation also depends on laser pulse number. It has been reported that laser ablation in a nitrogen environment can prepare a rough PDMS surface. Superhydrophilic trap-based surface is also prepared by using carbon dioxide laser on a glass substrate. But, it does not sustain long as a superhydrophilic surface after laser ablation. However, in extreme humid condition, the superhydrophilicity could be extended. Titanium oxide is used as a substrate for making superhydrophilic surface by applying laser [44].

4.1 Roughness

In this research a nanosecond pulsed laser is used under an ambient condition at the room temperature 25⁰C. The topography of the laser ablated surface was characterized by a scanning electron microscope (SEM, Helios Nano Lab 400, FEI, Hillsboro, OR). Round shape micro-grooved is observed as predicted from the nanosecond laser property analysis (Fig. 16). In the 1st experiment, 83% laser pulse overlap and laser pulse number 5 were used, where, the laser fluence was fixed for all the experiment as 2.96 J/cm². In this case, laser pulse steps were 50 μm.

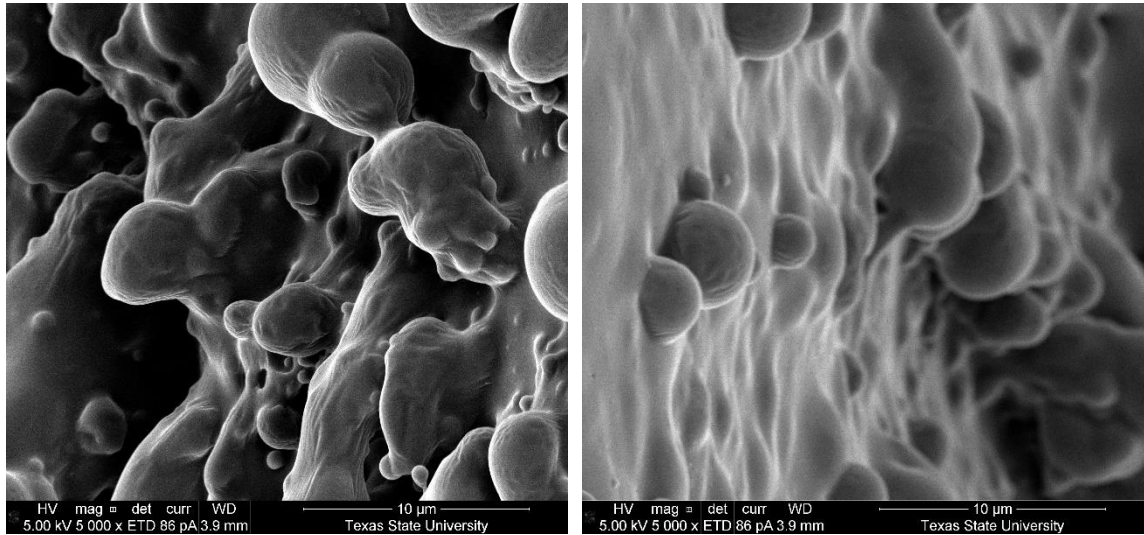


Fig. 16. Rounded micro-grooved formation in an air medium

It is observed that uniform surface roughness was formed by the laser ablation. Different shapes of the microchannel was fabricated for the capillary dynamic characteristic observation. A single channel and multichannels have different activity, where, single-channel carries a smaller amount of liquid rather than multichannel (Fig. 17).

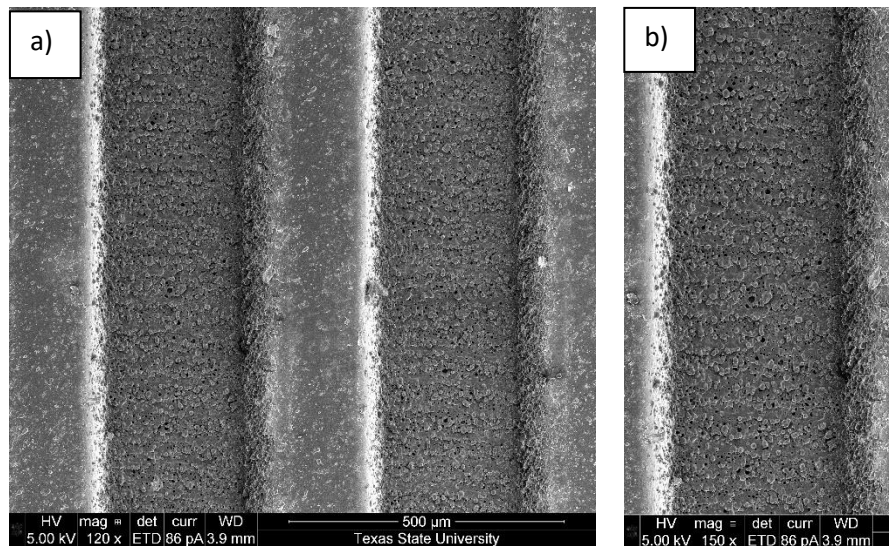


Fig. 17. a) Multichannel

b) Single channel

Surface roughness was measured inside the channel on an area of $100\ \mu\text{m} \times 100\ \mu\text{m}$ by using a stylus surface profiler (P-7, KLA Tencor, Milpitas, CA), which provided the

arithmetic mean RMS (Sq) value of surface roughness based on the 3D profile obtained (Fig.18 and19). The profilometer image shows that $70 \pm 5 \mu\text{m}$ depth cut has taken place by the laser ablation. Hence, different wide of the single channels such as $343 \mu\text{m}$, $444 \mu\text{m}$, $560 \mu\text{m}$ and $671 \mu\text{m}$ were also fabricated by maintaining same depth in the channel for this experiment.

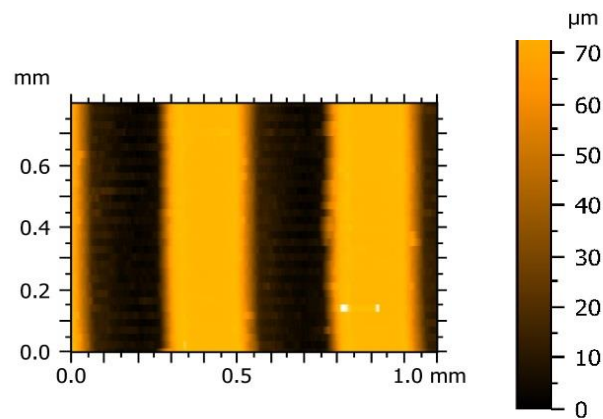


Fig. 18. Profilometer image

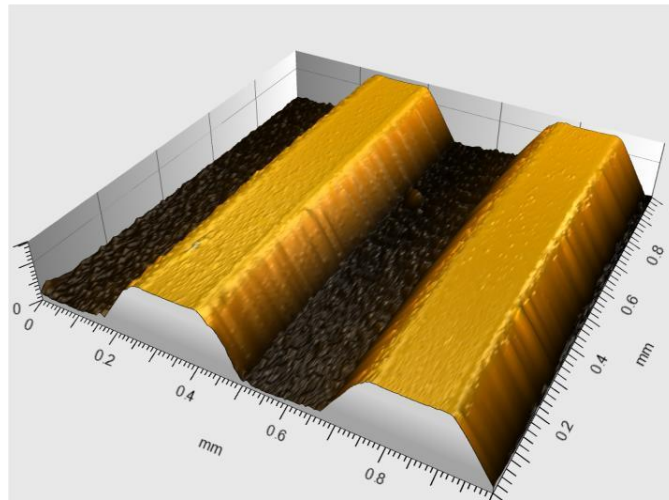


Fig. 19. Isometric View

In the 2nd experiment, the laser pulse number stayed fixed, but laser pulse step was changed as $50 \mu\text{m}$, $65 \mu\text{m}$, $80 \mu\text{m}$, $95 \mu\text{m}$, $110 \mu\text{m}$ and $125 \mu\text{m}$. So, the overlap

percentage changed as 83%, 78%, 73%, 68%, 63% and 58%. Since the overlap percentage changes the surface roughness also changed, which is shown in Fig. 20.

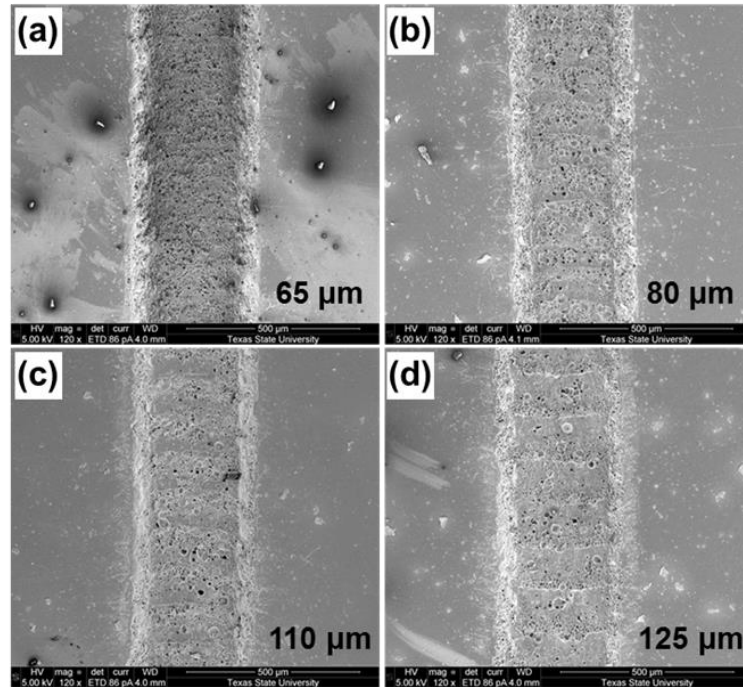


Fig. 20. Surface morphology by different laser pulse steps of 65 μm , 80 μm , 110 μm , and 125 μm in the y-direction.

4.2 Surface Chemistry Analysis

It is found that the high thermal ablation breaks the intermolecular bond and reacts with the air. As a result, some molecular bonds (-C-O-, C=O) [45] have formed on the top of the PMMA substrate, which attracts the water molecules. Under the high laser fluence of nanosecond laser, the photothermal effects are of significance and can be explained by the intense heating of work material. When a laser irradiates the substrate and subsequently causes the thermal breakdowns, there is the ejection of molten materials from the surface. To observe the presence of oxygen molecules on the substrate, XPS result has been taken. High pick is observed in the binding energy 532 and 533 eV, it

represents the presence of C=O, C-O bond on the PMMA surface. The Figure shows that with the increase of laser pulse number the presence of oxygen free radicals also increased.

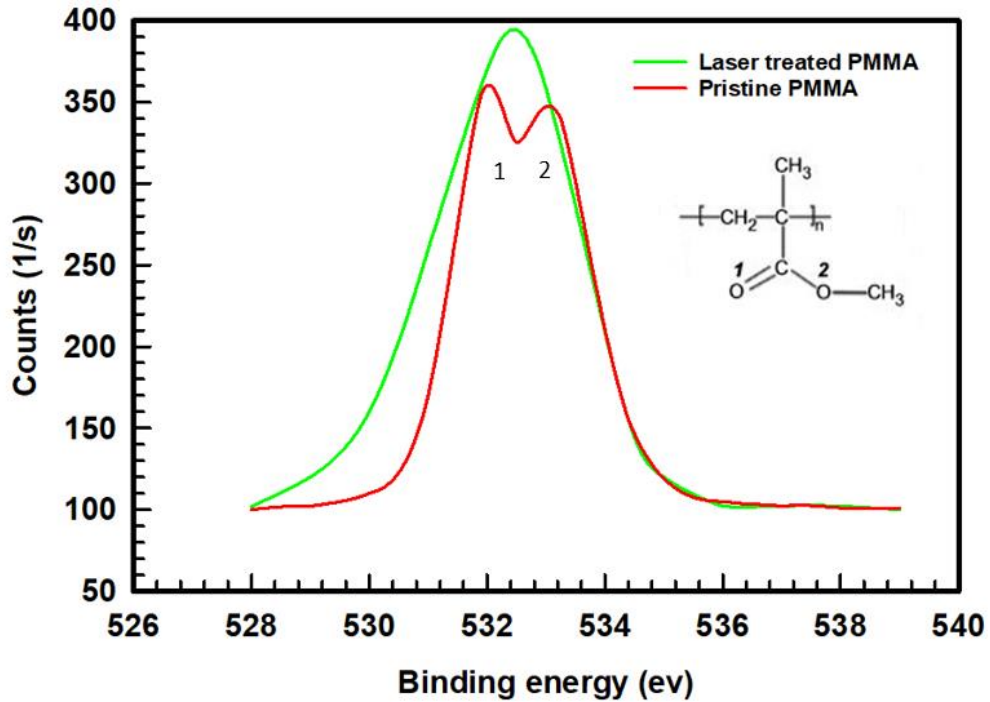


Fig. 21. Oxygen free radicals

4.3 Contact angle

The contact angle of a sessile water droplet, and surface tension of a pendant water drop, was measured using a contact angle and surface tension measurement instrument (Falcon, First Ten Angstroms, Inc., Portsmouth, VA). After dropping a DI water droplet of 5.52 μL onto the laser treated reservoir using a syringe. It is observed that, with the increase of laser pulse number, surface roughness increases and contact angle decreases. The reason behind that the higher amount of laser pulses caused more

irradiation on the PMMA surface, where the growth of surface roughness indicates more microgroove was formed during the laser scanning. On the other hand, contact angle depends on surface roughness, which, has been known from the Wenzel [46] equation $\cos \theta = r \cos \theta_E$, where θ_E is the pristine PMMA contact angle and r is the surface roughness parameter. Surface roughness contributes to increasing the surface energy with the increase of surface area, and it helps reduce the solid-liquid interfacial tension and to spread the liquid on the laser irradiated PMMA substrate by decreasing the contact angle. Hence, both surface chemistry and surface roughness contributes to making the surface superhydrophilic ($\theta < 5^\circ$) where the water contact angle reduced from 80° to 4.79° (Fig. 22).

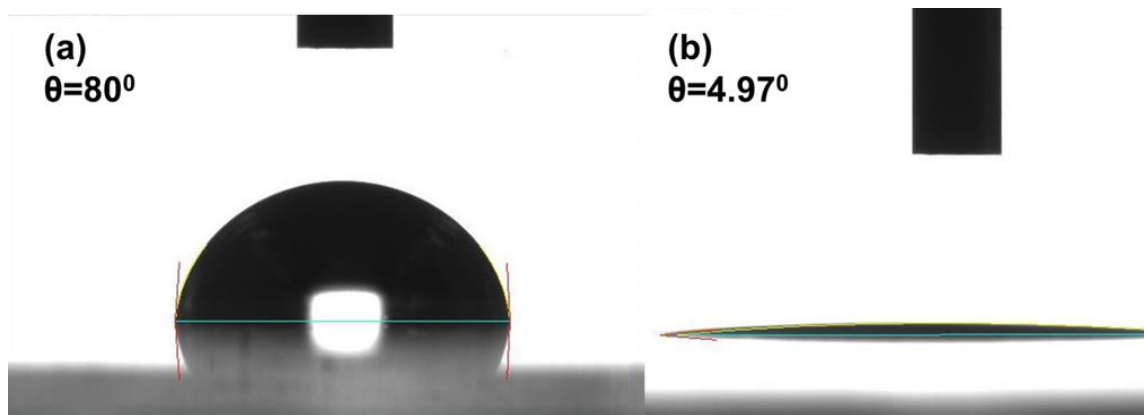


Fig. 22. a) Before laser treatment; b) Right after laser treatment

Though the surface roughness and surface chemistry rendered the surface superhydrophilic; however, hydrophobic recovery took place after 1 hour of laser ablation (Fig. 23). It is the natural phenomenon that surface molecules always try to stay in equilibrium energy state. When the laser ablation takes place, it produces oxygen based functional group on the top of the surface. In high-temperature, the laser breaks the carbon- oxygen bond and it creates oxygen free radicals which attract the water

molecules. After 1 hour of laser ablation, the polar groups produced during the surface oxidation tend to move into the bulk of polymer material under the room temperature and open-air system. However, they remain on the surface as long as they are in contact with water or any other polar environment. This is the exact reason as to why the surfactant solution (Fig. 24) is used after laser ablation. The presence of surfactant polar group on the laser treated surface helps to remain surface superhydrophilic for the long-term period.

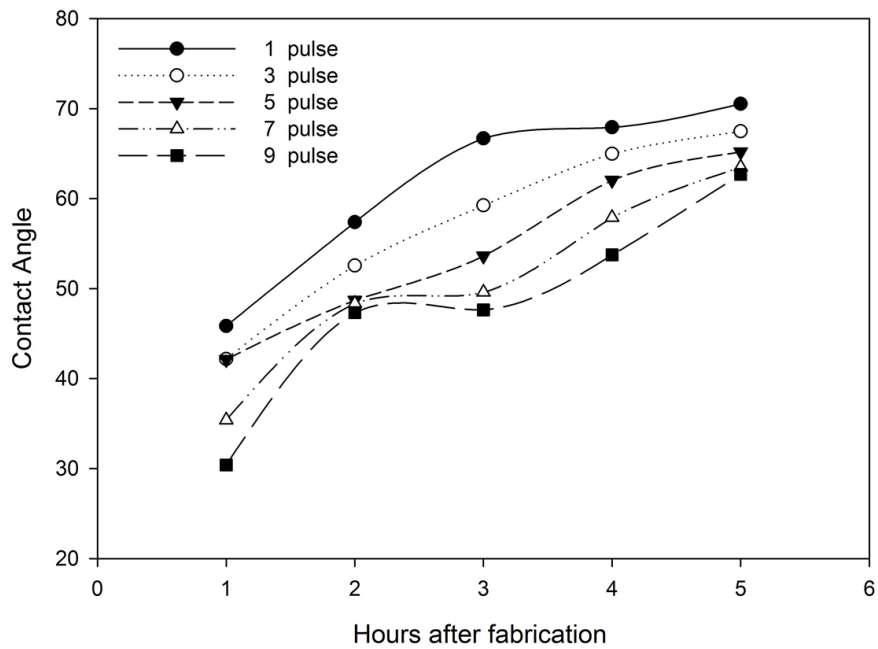


Fig. 23. Hydrophobic recovery after 1 hour of laser Ablation

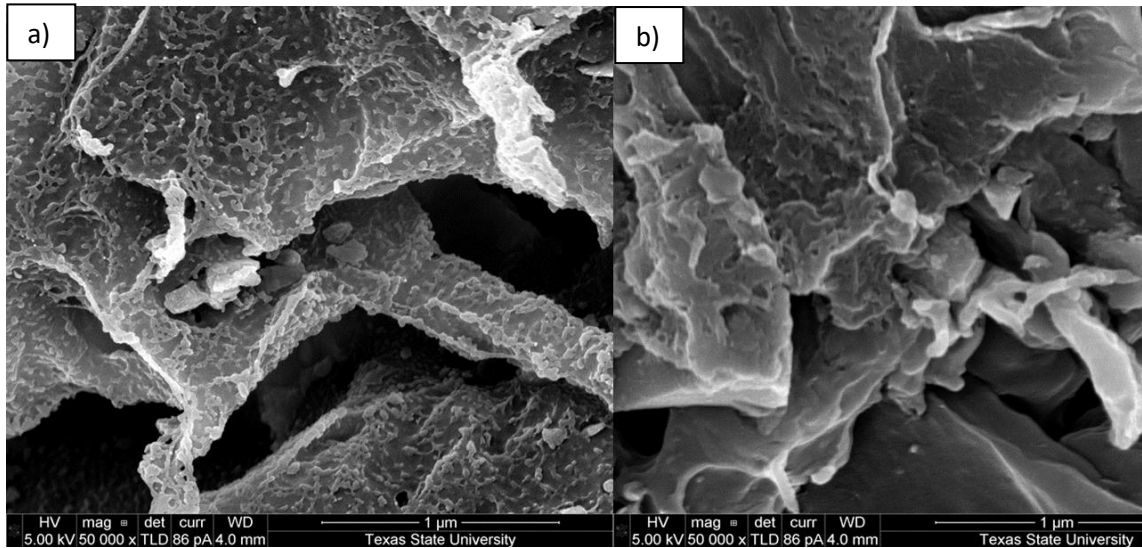


Fig. 24. a) Surfactant treated b) Without surfactant

4.4 Capillary flow rate

Generally, capillary flow takes place when the solid-liquid interfacial tension turns to greater than liquid gas interfacial tension. A particular setup is built to observe the capillary flow inside the laser ablated microchannel. The motion of meniscus along the microchannel was observed by using microscope equipped with a high-speed camera (NX4-S2, IDT Inc., Tallahassee, FL) (Fig. 25). Quantitative information was extracted from the acquired images using ImageJ software (NIH, Bethesda, MD). A 5.52 μL droplet of water and glycerol are used to observe the capillary driven flow.

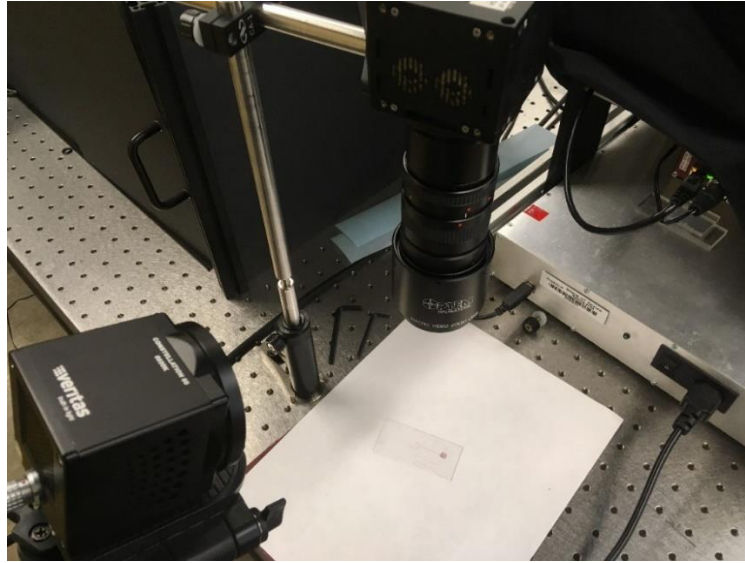


Fig. 25. Physical setup: High-speed camera

4.4.1 Water

After applying the water droplet on the top of the microchannel, the capillary flow is observed (Fig. 26). The different time elongation has been taken to see the character of the flow. The time scale was 80ms, and the position of the meniscus has been observed after every 50 images. The scaling of the meniscus position has been calibrated using millimeter scale and ImageJ software. In the image calibration, it is first need to take an image of the scale and to calibrate the particular distance between the two points using ImageJ software. Next, in the same focus and resolution, the meniscus's position was observed and measured in ImageJ software. In the case of this experiment, the calibration parameters were: 1mm = 40 (arbitrary unit). Different width of the channels (343 μm , 444 μm , 560 μm and 671 μm) were used for this experiment and result are shown in Fig. 27 where x^2 presents the displacement of liquid along the microchannel in respect to time t . For the open microchannel studies, we observed slower meniscus velocities in wider channels. It is found that, with the increase of channel width, the capillary driven speed decreased.

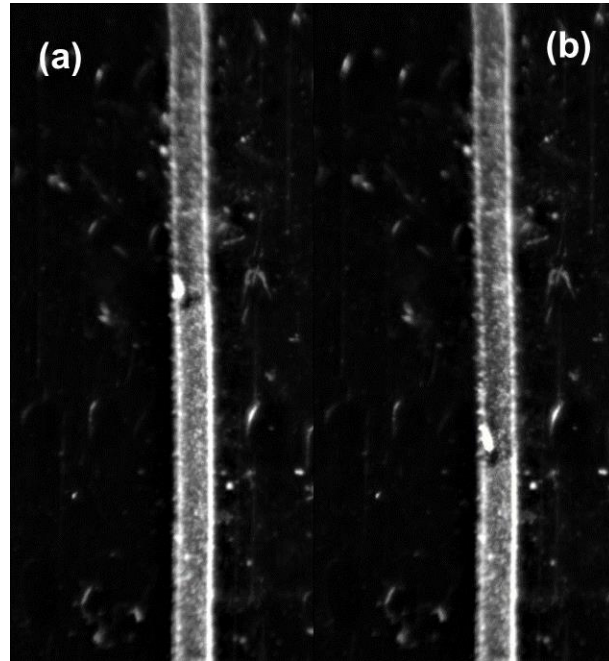


Fig. 26. Capillary Driven flow

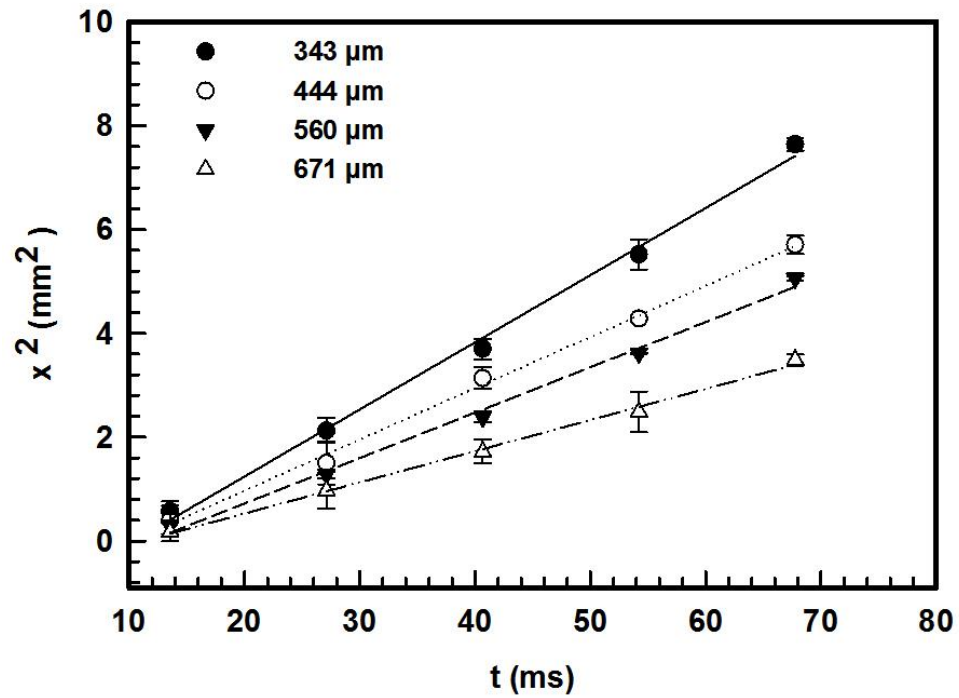


Fig. 27. Progress of the liquid meniscus, with time, t , corresponding to the different channel width. (RMS = 0.99).

4.4.2 Glycerol

Viscosity affects capillary driven flow. Highly viscous fluid means there is more force to work against the flow direction. Different volume concentration (20%, 40%, 60%) of viscous fluid (Glycerol-Water) mixture was used to see the interaction between laser ablated microchannel and the viscous fluids. Surface tension and viscosity were measured at the room temperature 23⁰C as shown in table 2 & Fig. 28.

Table 2: Different components and their liquid properties			
Components	Surface Tension (mN/m)	Viscosity (mPa-s)	Surface tension with (0.08M) AOT (mN/m)
Water	71.9 ± 1.12	.98 ± 0.02	26.12 ± 2.10
20 % of glycerol	65.98 ± 2.2	1.653 ± 0.072	21.31 ± 1.72
40 % of glycerol	62.27 ± 1.61	4.26 ± 0.05	18.10 ± 1.89
60 % of glycerol	57.74 ± 2.43	13.51 ± 0.22	15.21 ± 2.34

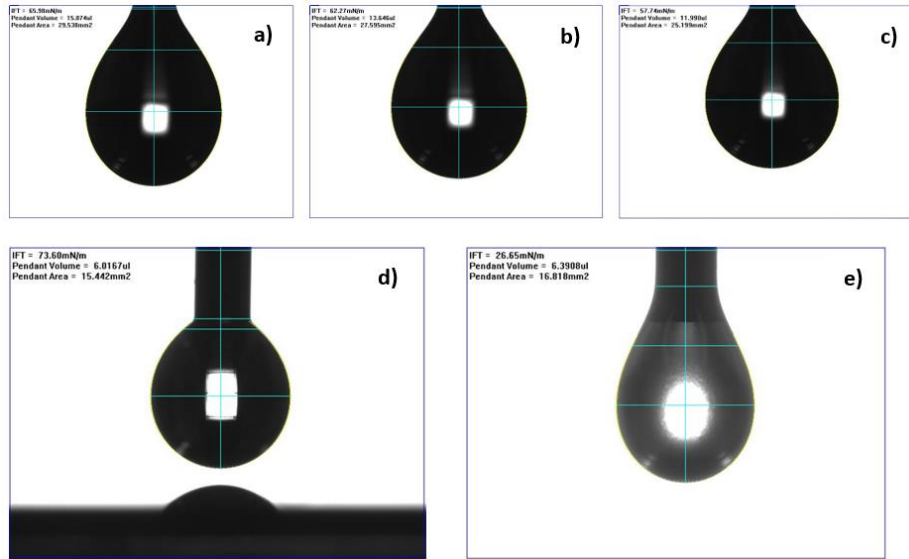


Fig. 28. a) 20 % glycerol-water b) 40 % glycerol-water c) 60 % glycerol-water d) DOI water e) surfactant-water solution surface tension measurement.

The result shows that the capillary flow rates with the increase of viscosity decreases as is shown in Fig. 29 where x^2 is the displacement of liquid. In the viscosity experiment, the same width of the channels ($444 \pm 5 \mu\text{m}$) were used to maintain the similar property of the microchannel for the all 3-different viscous fluids.

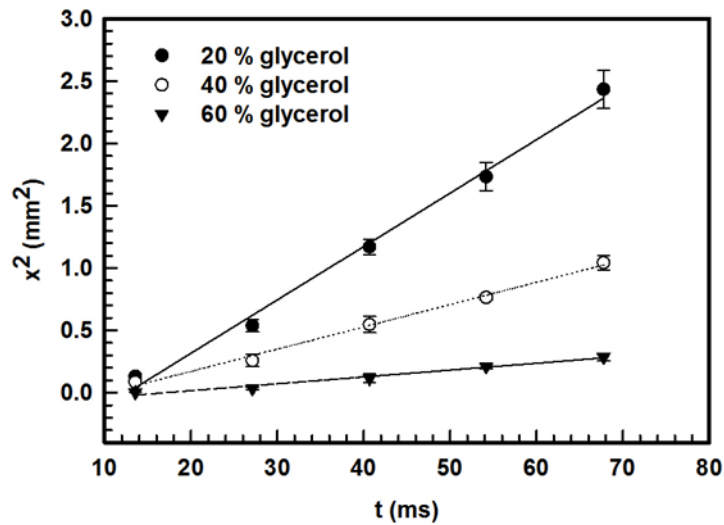


Fig. 29. Different viscous liquid with a channel width of ($444 \pm 5 \mu\text{m}$)

The capillary flow also can be controlled by changing the laser pulse steps in the Y direction. In addition, changing the pulse steps in Y direction indicates more morphological transformation inside the microchannel. Hence the different laser pulse steps (50 μm , 65 μm , 80 μm , 95 μm , 110 μm and 125 μm) of the channel are used to observe the flow character inside the channel. So, the corresponding overlap becomes 83 %, 78 %, 73 %, 68 %, 63 % and 58 %. The percentage of overlap indicates different roughness inside the ablated microchannel which has already shown in Fig. 20. Fig. 30, we see how the laser irradiation caused pulsed overlap.

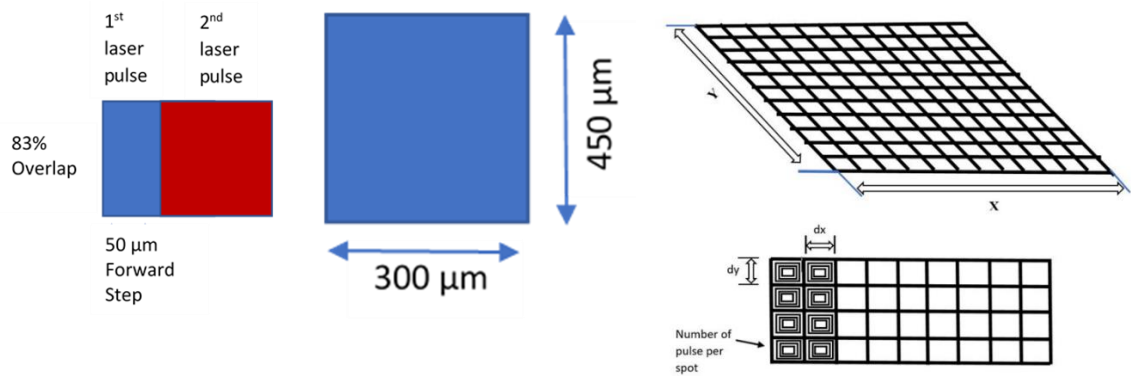


Fig. 30. Laser pulse overlap, dx (x directional laser movement), dy (y directional laser movement), the blue color shows the ablated area and the red color represents the 83% overlap of that blue color area.

As the pulse overlap has a direct relation with microgroove formation, we found with the increase of laser pulse overlap capillary driven speed increased. It means high pulse overlap is the responsible for higher surface roughness. Moreover, the high surface roughness caused more capillary driven flow inside the microchannel (Fig. 31).

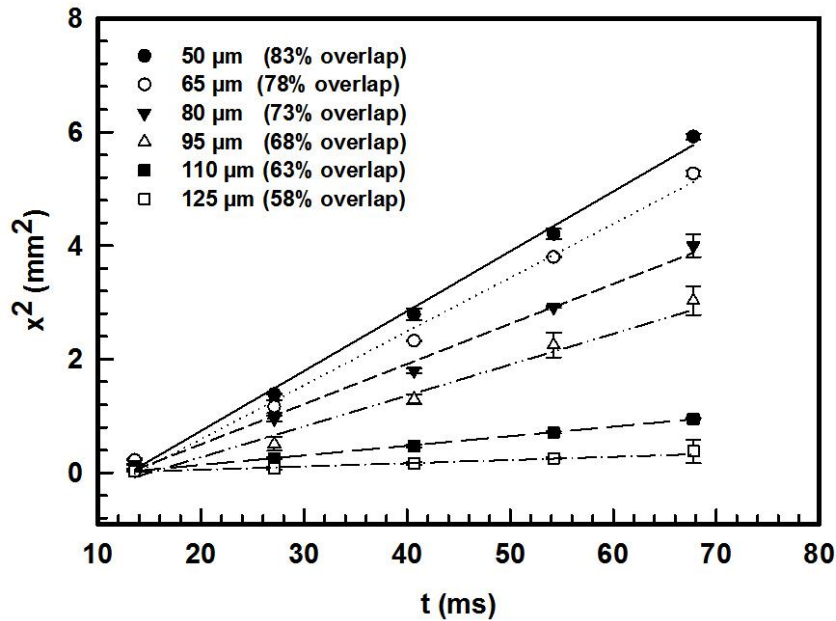


Fig. 31. In a fixed width ($W = 444 \pm 55 \mu\text{m}$), with the change of laser pulse steps capillary flow can be controlled and follow the governing equation ($R^2 = 0.99$).

Fig. 27, 29 & 31 represent that the capillary character inside the microchannel follows the Lucas-Washburn governing equation ($x^2 \propto t$). The plots have been drawn between the square distance that is traveled by the meniscus and the time that is needed for the meniscus to travel those distances. In every point, data have been taken in three times to get a statistical average. The R^2 value is 0.99 close to 1. In Fig. 31, It is interesting within a low capillary driven flow rate and non-uniform surface roughness, the flow still maintains the Lucas-Washburn [47] behavior. equation though some of the regions on the surface is over irradiated, and some of them are less irradiated. A barrier is observed between these two high and low contrast regions, which expectedly obstruct the capillary driven force and reduce the flow rate.

5. THEORETICAL AND EXPERIMENTAL ANALYSIS

5.1 Physics of capillary flow

The state of matter means the similar properties of molecular groups such as solid or liquid. Same states of material create a thin film of the boundary on the top of the surface due to cohesive force, this thin film is called the free surface. The attractive force of two similar types of molecules is called a cohesive force, whereas, the force between the two different molecules defined as adhesive force. Surface tension takes place due to cohesive forces existing between surface molecules in the liquid. The liquid molecule in the bulk of the liquid faced all direction of cohesive force, while, the surface molecule of liquid coheres only with the molecule in bulk and the neighbor in the surface. This strong attraction in bulk direction forming a thin film on the top of the liquid surface (Fig. 32).

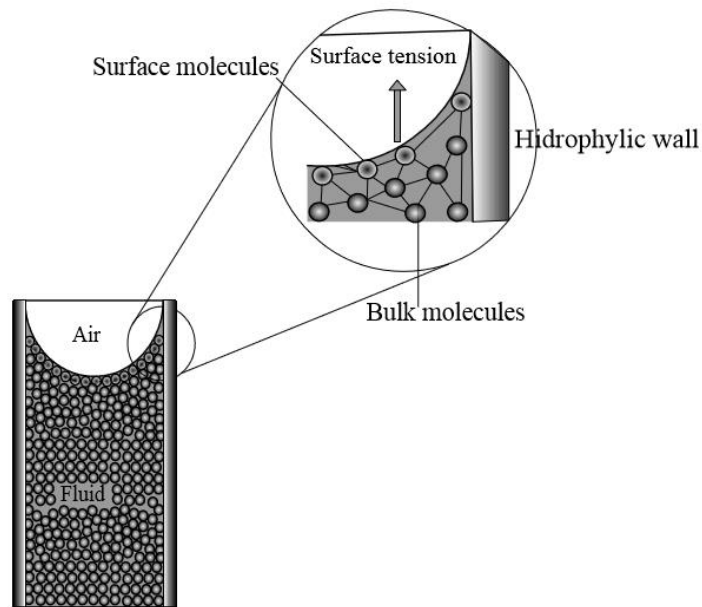


Fig. 32. Capillary force creation due to surface tension, [48]

The wall of the PMMA substrate which has used in this experiment is hydrophilic. As a result, there is an attraction force works between the wall and liquid and this force is an adhesive force. On the other hand, cohesive force tries to minimize the surface energy, and the meniscus turns to a concave shape. Finally, this adhesive force and cohesive force builds a force balance according to Newtons law. This force balance always depends on the surface wettability, and it helps move the liquid in the forward direction. As established equation shows that the distance traveled by the liquid is proportional to square root of time Lucas-Washburn equation. This flow dynamics equation does not consider the surface property. The experiment has been done in this research is entirely depends on surface morphology; hence it is necessary to establish an equation that takes account of surface morphology in the Lucas-Washburn equation.

$x^2 = kt$, where k is the dynamic coefficient

5.2 Theoretical model selection

5.2.1 Predicted model 1, for flow dynamics calculation

Using both Lucas-Washburn equation and Wenzel equation helps to model the capillary driven flow on the substrate. When a droplet of liquid is introduced on the substrate, it follows the Wenzel equation in the case of laser treated surface and the liquid move forward by following Lucas-Washburn behavioral equation (Fig. 33).

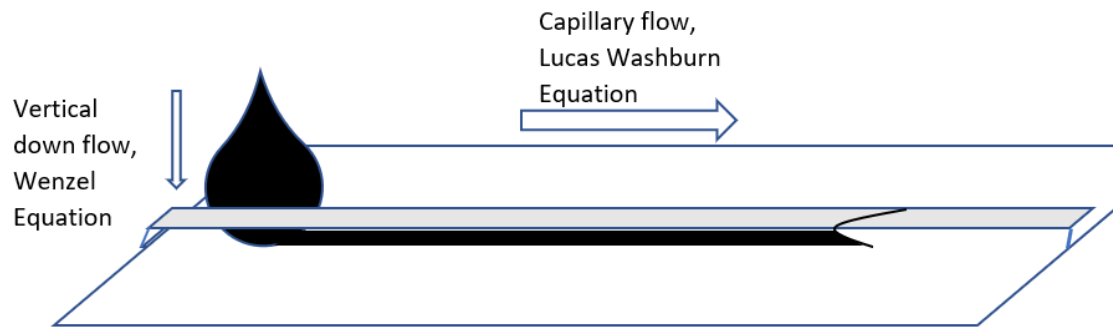


Fig. 33. Capillary driven flow and its behavior through the equation

The surface tension of the water droplet is reduced by adding surfactant solution, whereas the overall substrate energy remains higher than the liquid surface energy. This follows the Young's equation:

$$\cos\theta = \frac{\gamma_{sg} - \gamma_{sl}}{\gamma_{lg}}$$

By adding a surfactant, it is possible to reduce liquid gas interfacial tension (γ_{lg}). As a result, the contact angle will decrease and the liquid spread on the surface.

Furthermore, we see that it is possible to decrease the contact angle by increasing the roughness factor r , from the Wenzel equation

$$\cos\theta^* = r \cos\theta_E$$

Where θ_E is the pristine contact angle without any surface modification of the substrate and θ^* is the resultant contact angle after making the surface rough.

$$r = \frac{\text{Real surface area}}{\text{Projected surface area}} > 1$$

Since PMMA pristine contact angle, θ_E is 80° , a roughness factor that is estimated about 3.57 or above is needed to get a liquid contact angle less than 5° . The analytical formula of measuring roughness factor [49] is given by,

$$r = 1 + \frac{4dh}{(d + s)^2}$$

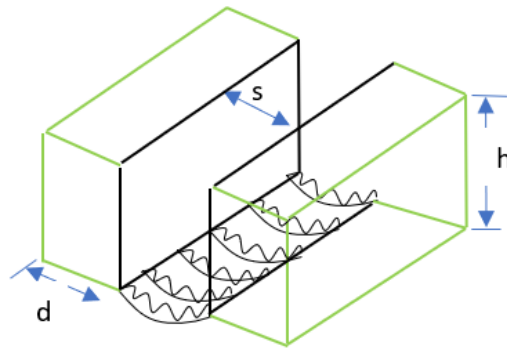


Fig. 34. Microgroove dimensions for the analytical formula of roughness factor, r

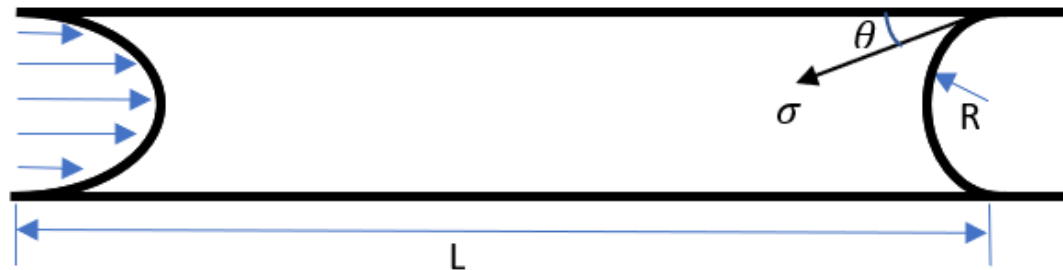


Fig. 35. Capillary flow and surface tension inside the channel

A fundamental process for the capillary flow is the ability of fluids to penetrate into fine pores with wettable walls. In this context, the filling of PMMA microchannel has found great importance. In a micro-channel of the circular cross-section with a radius r (see Fig.

35) filled with immiscible fluids, the meniscus can be approximated as a portion of a sphere with radius R, and the pressure difference across the meniscus is

$$\Delta p = 2\sigma/R \dots\dots\dots 1$$

The radius R of the meniscus will depend only on the contact angle θ and the radius of the channel

$$R = \frac{r}{\cos(\theta)} \dots\dots\dots 2$$

alternatively,

$$\Delta p = \frac{2\sigma\cos(\theta)}{r} \dots\dots\dots 3$$

The position of the meniscus x as a function of the time t when the two fluids considered have Newtonian behavior [50]:

$$x = \sqrt{\frac{r\sigma\cos(\theta)}{2\mu}} t \dots\dots\dots 4$$

Here, μ is the viscosity of the fluid. This equation assumes that the fluid is Newtonian with constant physical properties and that the flow is incompressible, steady and laminar.

The velocity of the meniscus which is assumed spherical with a constant radius of curvature [50] is:

$$V = \sqrt{\frac{r\sigma\cos(\theta)}{8\mu.t}} \dots\dots\dots 5$$

The significance of the gravitational force relative to capillary forces can be expressed using the Bond number (Bo):

$$Bo = \rho \gamma R^2 / g \dots\dots\dots 6$$

The Bo ranges between 0.06 and 0.31 for the liquids used in this study. Since the $Bo < 1$, the gravitational effect was considered negligible.

Reynolds number and Weber number are low for the studied system due to the lower surface tension and lower viscosity of the fluid.

$$We = \frac{\rho V^2 L}{\sigma} \dots\dots\dots 7$$

So, we can ignore those terms to calculate the capillary driven flow. Where V is a reference velocity, L is the characteristic length scale and σ is the surface tension coefficient, μ is the viscosity. Re and Bo are important non-dimensional numbers that help to understand the role of the forces in microfluidics:

- The Reynolds number is small. So, it is reasonable to assume that the viscous forces are dominant, and the flow is laminar.
- Bond number Bo defines the ratio between body and surface tension forces. The Bond number is small. This indicate that the surface forces are dominant and the body force like the gravitational force can be neglected while surface forces like surface tension play a fundamental role.

Where k is a Dynamic Coefficient dependent on the details of the particular system (including the channel cross-section and dimensions, and the viscosity and surface tension of the liquid).

The equation $x^2 \propto t$ can be derived numerically:

From Navier-stocks equation, considering the momentum equation in the x direction

$$\rho \left(\frac{\partial v_x}{\partial t} + v_x \frac{\partial v_x}{\partial x} + v_y \frac{\partial v_x}{\partial y} + v_z \frac{\partial v_x}{\partial z} \right) = - \frac{\partial P}{\partial x} + \mu \left(\frac{\partial^2 v_x}{\partial x^2} + \frac{\partial^2 v_x}{\partial y^2} + \frac{\partial^2 v_x}{\partial z^2} \right) + \rho g$$

The flow is steady with Non-Newtonian fluid and constant physical properties and there is only one nonzero velocity component in the x direction so that $v_y = v_z = 0$. Gravity force is in the negative y direction; hence, $g_y = -g$ and $g_x = g_z = 0$. This equation is simplified to

$$0 = - \frac{\partial P}{\partial x} + \mu \frac{\partial^2 v_x}{\partial y^2} \dots\dots\dots 9$$

If the dependence of pressure on y is neglected, then $P = P(x)$ is a function of x only.

Equation (9) becomes

$$\mu \frac{\partial^2 v_x}{\partial y^2} = \frac{\partial p}{\partial x} = \frac{p_2 - p_1}{L} \dots\dots\dots 10$$

A first integration gives

$$\frac{\partial v_x}{\partial y} = \frac{1}{\mu} \frac{\partial p}{\partial x} y + c_1 \dots\dots\dots 11$$

Since the velocity is a maximum at $y = 0$, we have

$$0 = \frac{1}{\mu} \frac{\partial p}{\partial x} (0) + c_1 \dots\dots\dots 12$$

$$C_1 = 0$$

A second integration of equation (14) with $C_1 = 0$ gives

$$v_x = \frac{1}{2\mu} \frac{\partial p}{\partial x} y^2 + C_2 \dots\dots\dots 13$$

The constant of integration C_2 can be obtained from the boundary condition that $v_x = 0$ at $y = h$.

$$0 = \frac{1}{2\mu} \frac{\partial p}{\partial x} h^2 + C_2 \dots\dots\dots 14$$

$$C_2 = - \frac{1}{2\mu} \frac{\partial p}{\partial x} h^2 \dots\dots\dots 15$$

Finally, the velocity profile is

$$v_x = \frac{1}{2\mu} \frac{\partial p}{\partial x} (y^2 - h^2) \dots\dots\dots 16$$

Assuming, $y^2 - h^2 = H$

$$v_x = \frac{1}{2\mu} \frac{\Delta p}{x} H \dots\dots\dots 17$$

$$\frac{\partial x}{\partial t} = \frac{1}{2\mu} \frac{\Delta p}{x} H \dots\dots\dots 18$$

From Laplace equation we get,

$$\Delta p = \frac{2\sigma \cos\theta}{H} \dots\dots\dots 19$$

By integrating the equation 18, we get the Lucas-Washburn equation:

$$x^2 \propto t$$

5.2.2 Predicted model 2, for flow dynamics calculation

How the channel depth and width affects the dynamic coefficient k was modeled mathematically. For the horizontal microchannel, capillary filling equation was derived by Bosanquet [51].

$$x^2(t) = \frac{2b}{a} \left(t - \frac{1}{a} \{1 - \exp(-at)\} \right) \dots\dots\dots 20$$

$$a = \frac{3\eta}{\rho H^2} f^{-1}(H, W) \dots\dots\dots 21$$

$$b = \frac{\gamma}{\rho H} \left[\cos\theta_c \left(1 + \frac{2H}{W} \right) - 1 \right] \dots\dots\dots 22$$

Where a and b are coefficients and derived from open microchannel with a rectangular cross-section geometry; η , γ , ρ is the liquid viscosity, surface tension, and density, respectively. H and W are channel depth and width, respectively, θ_c is the equilibrium contact angle, and f is a geometric function dependent on microchannel geometry: $f^{-1}(H, W) \approx 1 + 0.671004 (H/W) + 4.169711(H/W)^2$.

5.2.3 Predicted model 3, for flow dynamics calculation

To describe the capillary flow character and relationship between the channel morphology and capillary dynamics, an analytical model had been developed [52]. In the model capillary driving force is calculated from the change in the free energy of the system due to the liquid flow in the channel:

$$k = \frac{2\gamma h}{\mu} \frac{[2\cos\theta - (1 - \cos\theta)p]}{p^2} g(p) \dots\dots\dots 23$$

$$g(p) = \frac{128}{\pi^5} \sum_{n \geq 0} \frac{1}{n^5} \left[\frac{n\pi}{4} p - \tanh\left(\frac{n\pi}{4} p\right) \right] \text{ (full - slip) } \dots\dots\dots 24$$

$$g(p) = \frac{16}{\pi^5} \sum_{n \geq 0} \frac{1}{n^5} \left[\frac{n\pi}{4} p - \tanh\left(\frac{n\pi}{4} p\right) \right] \text{ (no - slip) } \dots\dots\dots 25$$

For $x^2 = kt$ where k is the dynamic coefficient which depends on channel depth (D) and width (w) and aspect ratio ($p = w/D$), surface tension (γ), contact angle (θ), and dynamic viscosity (μ). $g(p)$ is a geometric parameter that is dependent only on the channel cross-section.

For the multiple channel, flow can be divided (Fig. 36):

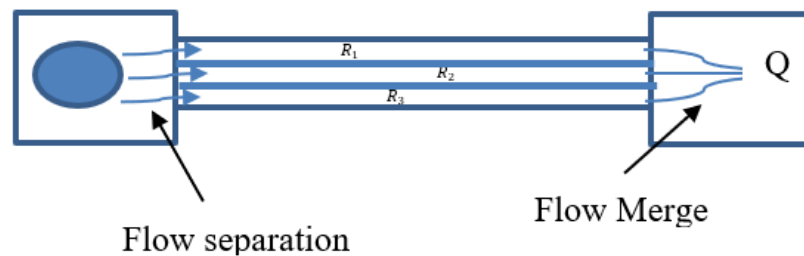


Fig. 36. Flow separation and merge in the multiple channels

$$x^2 \propto t \dots\dots\dots 26$$

$$x^2 = k\gamma t \text{ [We can write the constant } k\gamma]$$

$$\frac{\partial}{\partial x}(x^2) = \frac{\partial}{\partial x}(k\gamma t)$$

$$2x \frac{\partial x}{\partial t} = k\gamma ;$$

$$v = \frac{k}{2x} \gamma ;$$

$$v = \frac{Q}{wh} = \frac{k}{2x} \gamma ;$$

Q volumetric flow rate, γ = surface tension, w= channel width, h = channel height.

$$Q = \frac{kp h^2}{2x} \gamma;$$

From young's equation:

$$\cos(\theta) = \frac{\gamma_{sg} - \gamma_{sl}}{\gamma}; [\gamma_{sg} = \text{Solid gas interfacial tension, } \gamma_{sl} = \text{Solid-liquid interfacial tension.}]$$

$$\gamma = \frac{\gamma_{sg} - \gamma_{sl}}{\cos(\theta)};$$

$$(\gamma_{sg} - \gamma_{sl}) = Q \times \frac{2x \cos(\theta)}{kp h^2};$$

For the multiple channels, the flow rate will be:

$$\gamma_{sg} - \gamma_{sl} = RQ \quad [\text{Where } R = \frac{2x \cos(\theta)}{kp h^2}]$$

R is the flow resistance.

Multiple channel resistance R_1, R_2

$$\frac{1}{R_C} = \frac{1}{R_1} + \frac{1}{R_2}$$

The different mathematical model are compared to each other. The movement of the liquid is much slower in the Model 1 & 2. However, in the case of model 3, the displacement of the liquid is much higher than any other model. The reason is that the equation of the model 3 is derived from the surface free energy system. With the increase of surface roughness, surface energy is increased. As a result, the model 3 is accounted

for this research, and the theoretical results have been compared with the experimental result.

5.3 Theoretical and experimental result comparison

It has been already discussed that model number 3 is good to count for this research. By putting the theoretical and experimental value together in the plot, we may compare the result. In the plot, dynamic coefficient k is compared with the channel aspect ratio $p=w/D$; where w and D are the channel width and depth, respectively.

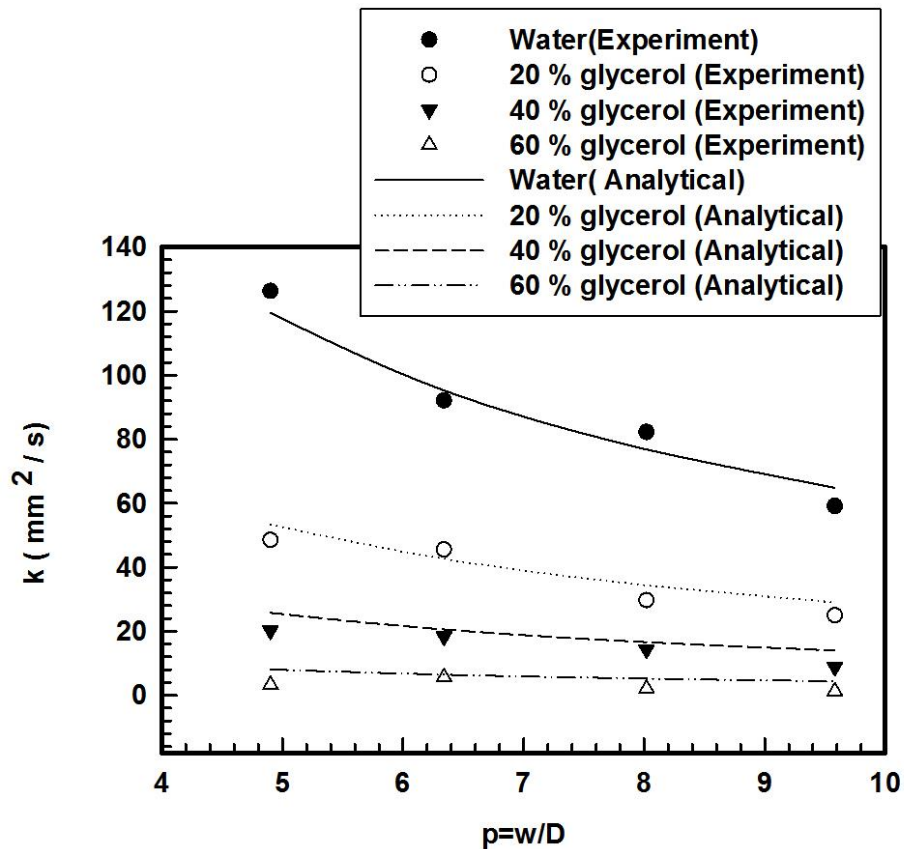


Fig. 37. Theoretical and experimental comparison of the dynamic coefficient (k) with the no-slip boundary condition.

Experiments have been carried out on laser and surfactant treated PMMA surfaces. Fig. 38, shows theoretical and experimental results. In the calculation of the dynamic

coefficient k , a constant and complete capillary filling by liquid has been assumed. As the surfactant layer does not permanently inhabit with the channel wall, so the liquid droplet mixed with the surfactant during the capillary filling thus reducing the liquid surface tension. In this case, we assumed the DI water surface tension is equivalent to the surface tension of surfactant-water mixture. Similarly, the surface tension of glycerol-water mixture could be equal to the surface tension force of water-glycerol-surfactant mixture. Hence, we individually calculate the surface tension forces and viscosity to estimate the theoretical result which is shown in table 1. Fig. 38 also shows that k value decreases with the increase in viscosity. The viscosity has a direct impact on dynamic coefficient k as expected. In the highly viscous fluid, the less value of dynamics coefficient k is observed. The theoretical and experimental results are close to each other under the no-slip boundary condition. In the no-slip boundary condition, slower movement of fluid was observed in the contact line of meniscus on channel wall when high viscous liquid was used. It is plausible because immobilization takes place in the channel wall due to the presence of surfactants. Gradual reduction of the dynamic coefficient (k) is also observed in the case of increasing the channel aspect ratio (p). In this research, the experimental capillary driven flow is too high that we can neglect the dynamic contact angle and only accept the static contact angle. The liquid-air interface is relatively flat what we assumed before the experiment, and it proves from the observation of small curvature of the liquid-air interface. Also, the meniscus shape changed during the capillary filling. In the high aspect ratio (p) meniscus never maintains constant in shape (Fig. 38).

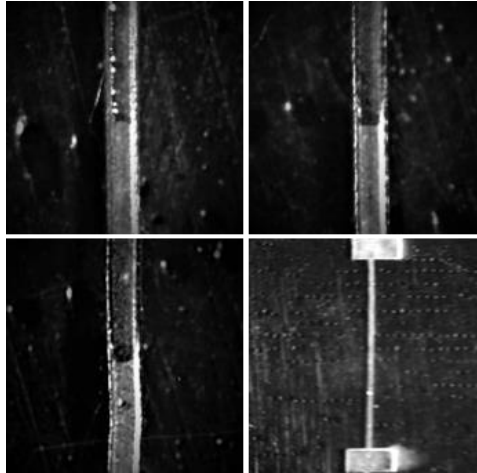


Fig. 38. Meniscus shape changes during the capillary flow

Nevertheless, it has little effect on our dynamic coefficient (k) calculation in the case of high-speed capillary driven flow. It also should be noted that, the geometric shape factor $g(p)$ was derived for the rectangular shape of the channel. No governing $g(p)$ equation of arbitrary channel shape exists. The fabricated device is close to a rectangular shape (Fig. 39), though the thermal ablation does not provide the perfectly rectangular shape channel. Hence, the dynamic coefficient k is close to the theoretical assumption for rectangular shape microchannel in no-slip boundary condition (Fig. 40), and the result is quite acceptable.

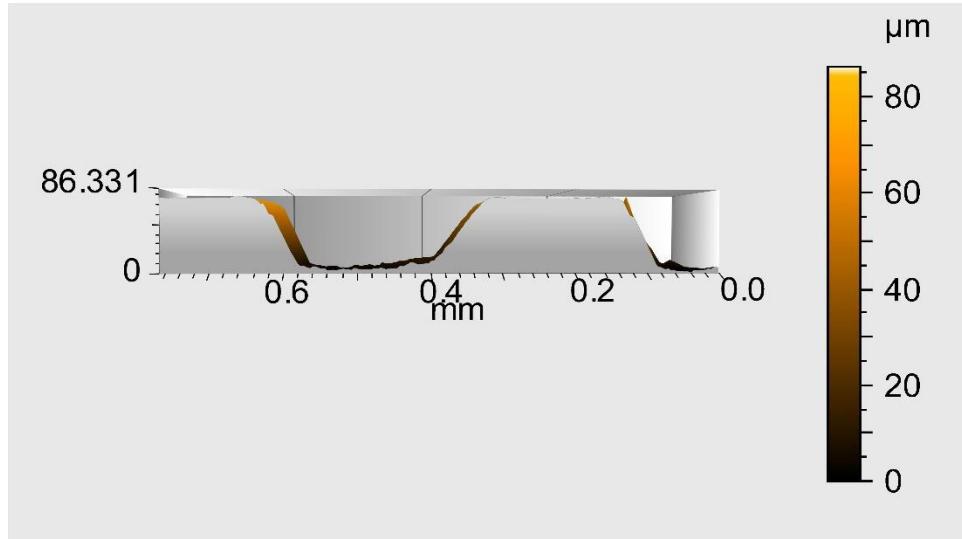


Fig. 38. Cross section of the microchannel (80 μm depth)

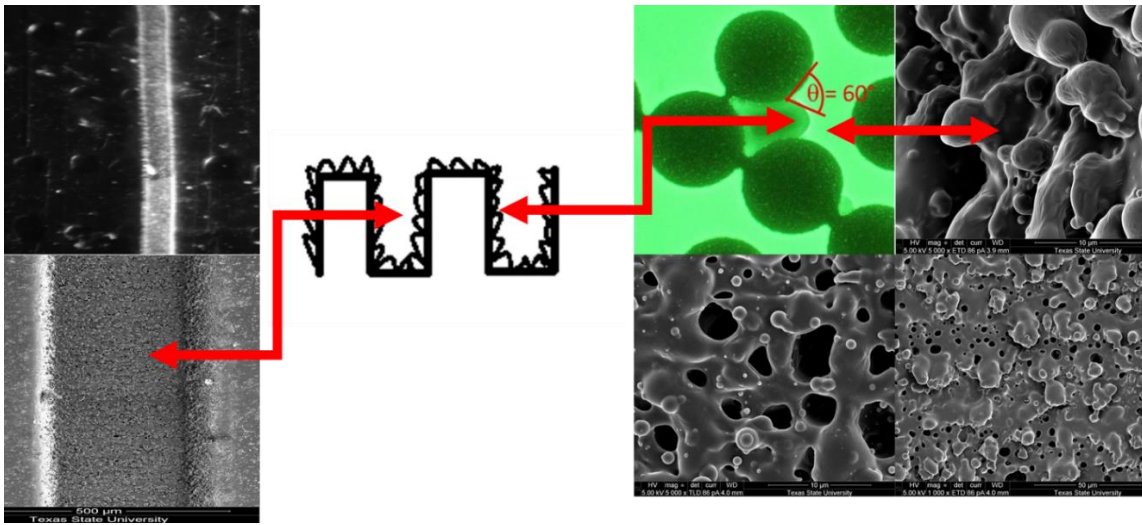


Fig. 40. Multiscale rough surface fabrication via laser irradiation and corresponding capillary driven flow, Helmut et al, (The impact of pore structure and surface roughness).

6. ASSAY PREPARATION

Surfaces with micro and nanostructure contain unique properties, that could be applied in biomedical and tissue engineering applications. In the previous sections, the thermoplastics polymers are converted to capillary driven devices, where the surface structure was rough. A nanostructure was created inside the microchannel using laser ablation and surface chemistry was modified using surfactant solutions. This section of the thesis contains lateral flow assay fabrication procedure where the biomolecules is applied on laser modified surface. The assay depends on surface morphology and surface chemistry. There are several important points we need to note for fabrication of polymer substrate to be used for lateral flow assay, such as protein immobilization, test device fabrication, and detection particle choice.

Proteins are biomolecules that play essential roles for cellular information exchanges. Protein states are useful indicators of disease response to treatment. Immobilization method depends on protein and surface property. One of the simplest surfaces, on which protein is immobilized is the inner surface of microfluidic channels. There are two types of surfaces that are used for protein immobilization: Planar surface and 3d surface. The planar surface contains silicon, glass, PDMS, plastic and Metal. Silicon is the commonly used material, but less transparent for the microfluidic application. Glass is good for saline based immobilization, but not flexible. PDMS and plastic materials have a hydrophobic character, which is the primary drawback of protein absorption. Metals films are seldomly deposited on silicon or glass surface and protein is immobilized on the metal surface for detection methods other than fluorescence or colorimetric detection, but the addition of protein is labor intensive. For the case of three-dimension materials

packed bead beds, hydrogel, sol-gel, porous polymer monolith, membranes and paper are used. In this research, a roughed PMMA substrate is used which has been fabricated by applying laser thermal ablation.

A wide variety of immobilization methods are used to attach protein on the surface.

Ideally, active sites for antibody binding or enzymatic conversion should be accessible to reaction partners. The most straightforward method for protein immobilization is physical absorption. In this process, protein adsorbed to the surface via intermolecular force such as electrostatic, Vander Waal's, and hydrophobic interaction. Protein is not stable in the case of covalent binding. Basically, intermolecular force depends on pH condition of the environment [53]. The pH of a solution can have several effects on the structure and activity of enzymes. For example, pH can have an effect on the state of ionization of acidic or basic amino acids. Acidic amino acids have carboxyl functional groups in their side chains. Basic amino acids have amine functional groups in their side chains. If the state of ionization of amino acids in a protein is altered then the ionic bonds that help to determine the 3-D shape of the protein can be altered. This can lead to altered protein recognition or an enzyme might become inactive. Therefore, immobilization of protein can be difficult using physical absorption process.

In the case of electrostatic interaction, the functional groups are involved in protein and a surface. Complete isolation from other intermolecular forces is impossible.

Intermolecular force acts when nitrocellulose and Polyvinylidene fluoride membrane is used as a substrate. Protein immobilization on nitrocellulose membrane is work primarily to hydrophobic interaction which benefits from porous morphology as well as

localization in a specific region [54]. Owing to the small pore sizes, protein can be effectively encapsulated.

In this research, a PMMA microfluidic device has been designed in SolidWorks before going to develop the assay (Fig. 41). There are sample reservoir, test line, and wicking reservoir. The droplet is dropped inside the sample reservoir via syringe. In the test line, the antibody-antigen reaction takes place, and the wick works as a suction chamber for the rest of the liquid.

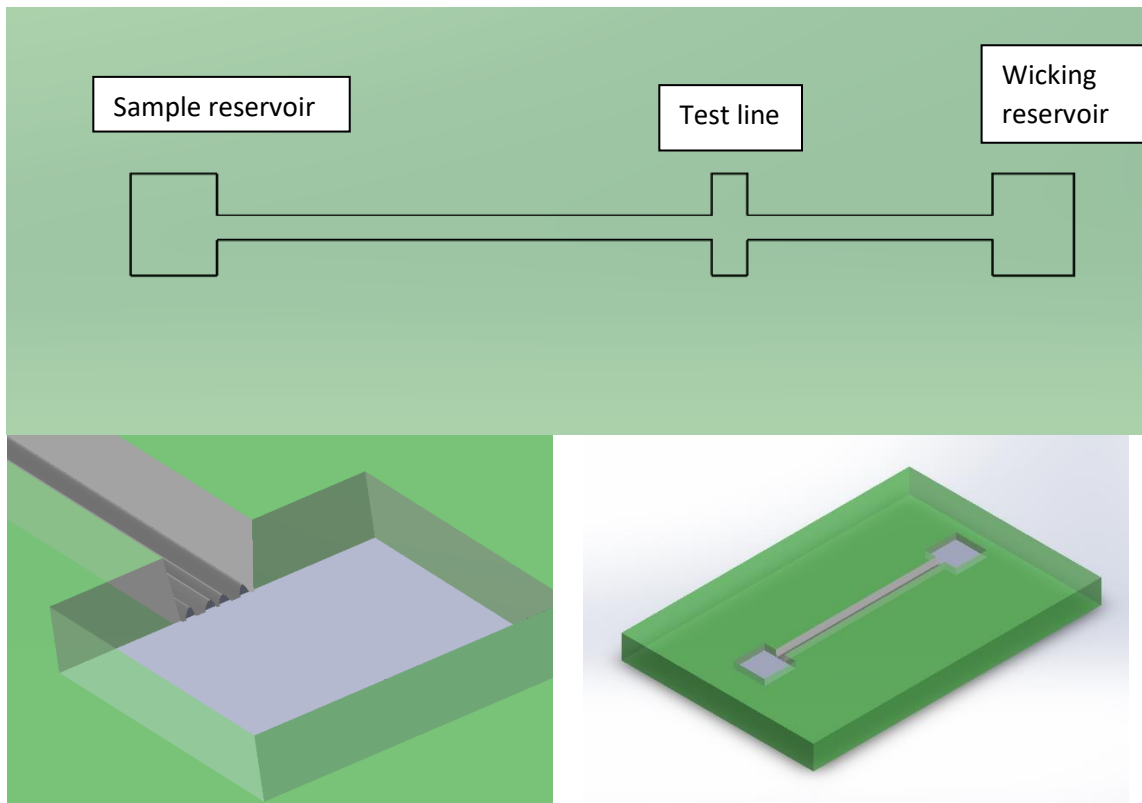


Fig. 41. Solid works modeling PMMA device

6.1 Device fabrication

6.1.1 Reservoirs

Nanosecond laser is applied on the PMMA substrate with a rectangular area $4\text{ mm} \times 4\text{ mm}$. In the ablation, the laser repetition and fluence were 10 and 2.96 j/cm^2 , respectively. X and Y directional laser pulse step was $100\text{ }\mu\text{m}$ and the pulse number was 5.

6.1.2 Channel formation

A single line channel was formed due to maintaining the aperture size $300\text{ }\mu\text{m} \times 450\text{ }\mu\text{m}$. The width of the aperture was $450\text{ }\mu\text{m}$ as a result, the channel which formed due to laser ablation was $444\text{ }\mu\text{m}$ wide. Laser pulse number of 5 and Y directional steps of $50\text{ }\mu\text{m}$ were used, and it creates an $80\text{ }\mu\text{m}$ deep inside the channel.

6.1.3 Test line formation

A test line is a place, where antigen and antibody reaction take place. A $1.5\text{ mm} \times 4\text{ mm}$ test line was fabricated on the top of the microchannel. Unique laser ablation has been done in the test line area. For the channel, test line and reservoir fabrication, laser pulse number 5 was used where the laser pulse step was $100\text{ }\mu\text{m}$ in X and Y direction. The secondary laser ablation was also applied to the test line maintaining the laser pulse steps and pulse number $500\text{ }\mu\text{m} \times 500\text{ }\mu\text{m}$ and five subsequently (Fig. 42). The secondary laser ablation creates a tiny hole inside the test line in the specific pattern which helps to trap the antibody inside the test line.

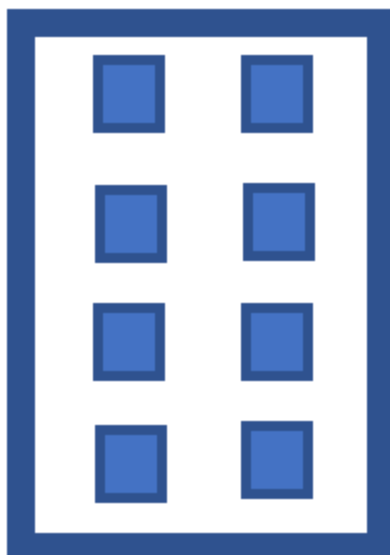


Fig. 42. Multiple laser ablation and pillar creation.

6.1.4 Wicking reservoir

The wick reservoir is an area where the rest of the liquid will be reserved: the liquid which was not used in a chemical reaction in the test line. The wicking reservoir was also same as reservoir size.

6.2 Solution preparation

Biotinylated BSA and Streptavidin Coated Gold nanoparticles were purchased from Sigma Aldrich. Albumins are readily soluble in water and can only be precipitated by high concentrations of neutral salts such as ammonium sulfate. However, albumin is readily coagulated by heat; when heated to 50°C or above, albumin quite rapidly forms hydrophobic aggregates which do not revert to monomers upon cooling. Two different concentrations of BSA solution (1.52% & 11.68% of the water and BSA mixture) was prepared by fixing the gold nanoparticle concentration.

6.3 Protein immobilization and characterization

The fabricated PMMA surface was highly rough after laser ablation, especially the test line where the multiple laser ablation was done. To introduce more functional group inside the test line oxygen plasma was used for 10 minutes and 20 minutes. After applying the oxygen plasma, the surface turns to more hydrophilic. Immediately, the BSA solution was applied to that region by blocking the other area. Then the device is put in the oven at 40⁰C for the dry purpose for 2 hours. Due to plasma application, the surface molecules introduce more functional (-C-O- and -C=O) group on the top of the surface which makes the surface superhydrophilic. Hence, BSA molecules absorb by the surface due to the surface roughness and superhydrophilicity.

After applying the BSA solution, the surfactant solution is added inside the channel and wicking reservoir without mixing it with the test line solution. Then again, the device is dry in the oven. For the test purpose and visual observation, 20 nm gold nanoparticle solution was used. Streptavidin has a high binding property with biotin. A single droplet of the gold nanoparticles were coated with streptavidin gold nanoparticle was applied to the sample reservoir of the microfluidic device and the solution moved inside the channel due to the capillary force. In the test line area, gold nanoparticle trapped by streptavidin biotin reaction and shows the color changes. The rest of the fluid which doesn't react flowed through the channel and reach the wicking reservoir. The presence of color changes represent the performance of the device. More color changes would be found for the more effectual devices (Fig. 43).

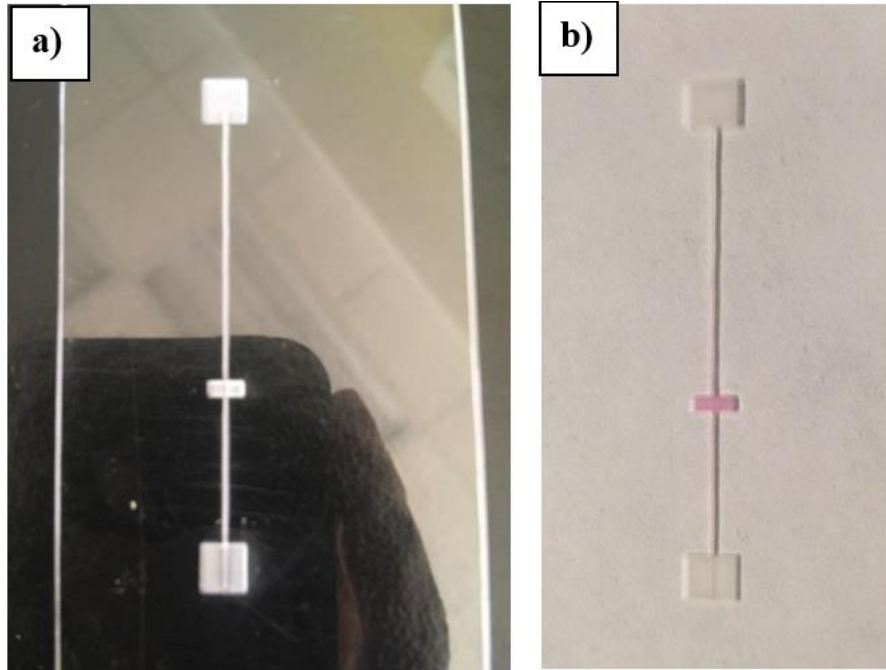


Fig. 43. a) Without antigen and antibody reaction b) Color change with the presence of antibody and antigen



Fig. 44. Left: Compact PMMA device, Middle: Nitrocellulose device, Right: PMMA device the possible replacement of Nitrocellulose membrane only.

7. CONCLUSION

In this research, some new strategies have been introduced for preparing the lateral flow assay device, which could lead to altering the contemporary LFIA manufacturing procedure. Laser micromachining has been done on a PMMA substrate in a controlled way to create the multiscale roughness. Laser pulse number 5 is an excellent fit for slight PMMA surface modification which provides sufficient transparency. Additionally, 50 μm pulse steps contain 83% overlap which is good for getting the uniform surface roughness that helps to ensure faster capillary flow inside the channel. Fluid dynamics of a capillary driven flow in a rectangular(almost) shaped was studied and the effect of surface roughness on the flow behaviour was identified in a laser ablated microchannel. It was observed that the capillary driven flow in the laser modified multiscale rough surface follows the Lucas-Washburn governing equation, which is developed for the smooth surface. Viscosity and channel aspect ratio plays vital roles in the capillary driven flow. In the case of high viscous flow, lower meniscus movement was observed, and it shows a good agreement with Lucas-Washburn equation. In the faster capillary flow regime, the smaller deviation was observed from the Luca-Washburn equation. It happens due to viscus effect where the high viscous fluid has much more interaction with the channel wall and the boundary condition has fell in the threshold of the no-slip boundary condition. This means the high viscous fluid is more controllable in the capillary driven flow. Moreover, the lower viscous liquid has less frictional interaction with the channel wall, so it moves faster and deviated from Lucas-Washburn governing equation.

The surface roughness creates a trap for surfactant absorption. So, it is not only helps with meniscus movement, but also helps to fabricate reusable PMMA device. Laser ablation changes the surface chemistry and surface morphology together. It is very convenient for protein immobilization where polarized attraction works between the protein solution and the carbonyl group on the laser-treated surface. Finally, it can be said that the laser modified PMMA substrate is suitable as an alternative material of nitrocellulose membrane. The laser modified surface does not only applicable to the lateral flow assay device, but also can be used in lab-on-a-chip where multiple channels can be used for the multiple tests.

APPENDIX SECTION

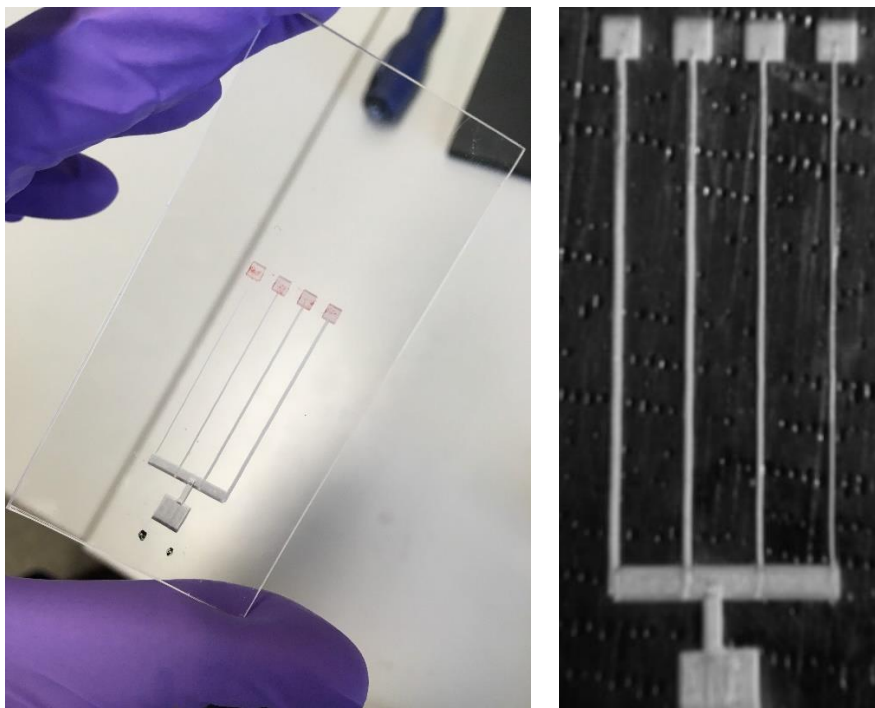


Fig. A1. Multiple channel fabrication using laser surface treatment for lab-on-a-chip fabrication.

Vertical flow test in different size of laser ablated microchannel:

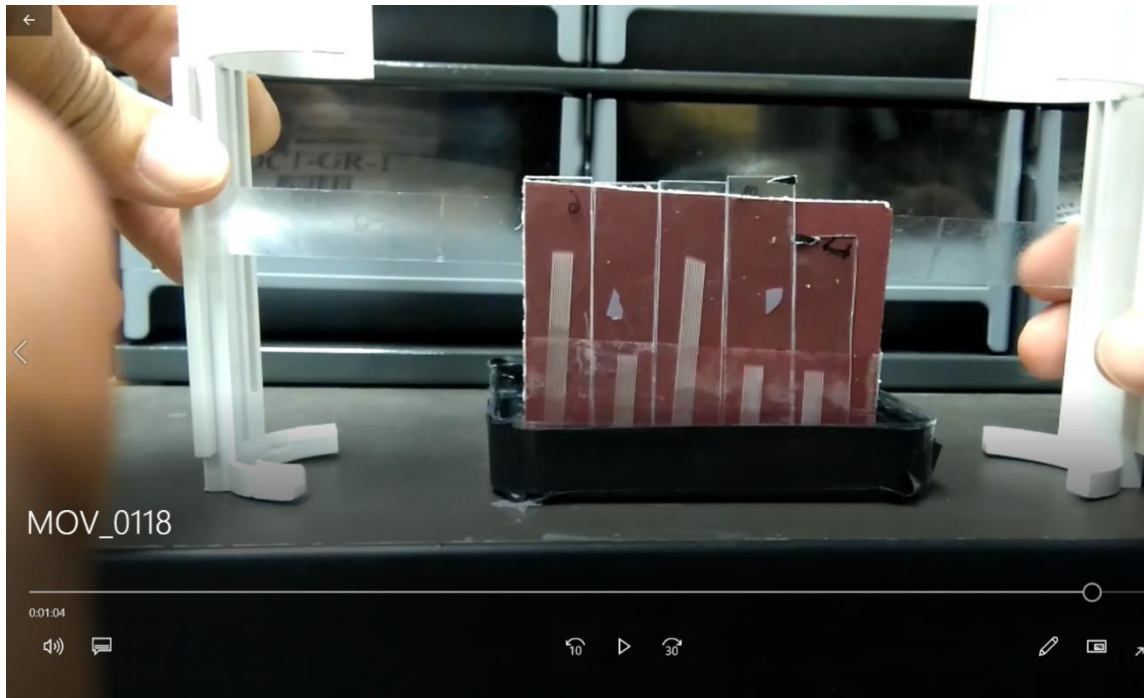


Fig. A2. Vertical capillary flow test

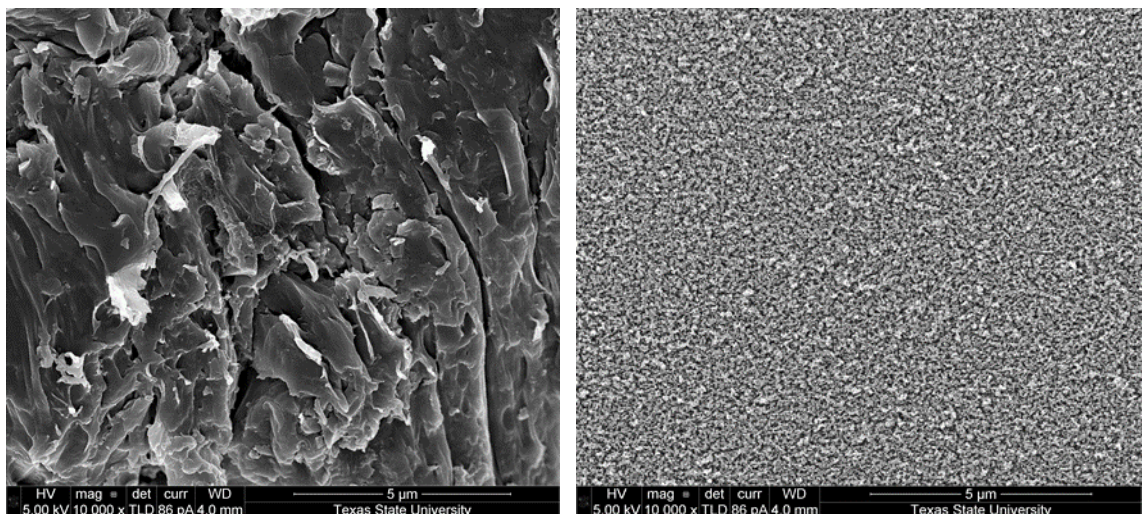


Fig. A3. Left: Sandblasted PMMA; Right: Laser treated Polycarbonate

MATLAB code:

```
clc,clear
format long;

%w=input(' w ');
%disp('input height');
%h=input(' h ');
w=343e-6;

h=70e-6;

%n=3;
%n=input('n ');
p=w/h;
x=0.078;
y=5;
%%L=p/(p+2);

z=0.00089;
L=z/x;
disp(L);
% x= surfcae tension, y= contact angle, Z=viscosity
sum1=0;
for i=1:2:1000
sum1=sum1+(16/pi^5)*(1/i^5)*(i*(pi/2)*p-tanh(i*(pi/2)*p));% no slip
end

disp( 'No slip sum1 ');
disp(sum1);
sum2=0;

for i=1:2:1000
sum2=sum2+(128/pi^5)*(1/i^5)*(i*(pi/4)*p-tanh(i*(pi/4)*p));% slip
end
disp( 'slip sum2 ');
disp(sum2);

k1= (2*h*(2*cos(pi*y/180)-(1-cos(pi*y/180))*p)/((p^2))*sum1; % kz/x
k2= (2*h*(2*cos(pi*y/180)-(1-cos(pi*y/180))*p)/((p^2))*sum2;

disp( 'No slip k1 ');
disp(k1*10^6);
disp( 'slip k2');
disp(k2*10^6);
disp(p)
```

Visual Basic code

```
'#####
####
'X Right = 0   X Left = 1
'Y Up = 0     Y Down = 1
'#####
####
```

```

$regfile = "XM256A3BUDEF.DAT"
$crystal = 32000000 '32MHz
$hwstack = 100
$swstack = 100
$framesize = 100
$lib "xmega.lib"
$external _xmegafix_clear
$external _xmegafix_rol_r1014
'----- OSC -----
Config Osc = Enabled , 32mhzosc = Enabled '32MHz
Config Sysclock = 32mhz , Prescalea = 1 , Prescalebc = 1_1
'$crystal = 32000000
'Config Osc = Disabled , Extosc = Enabled , Range = 12mhz_16mhz , Startup = Xtal_1kclk , 32khzosc
= Enabled
" Set PLL OSC conditions:
'Osc_pllctrl = &B1100_0010 ' reference external oscillator, set the PLL'
multiplication factor to 2 (bits 0 - 4)
'Set Osc_ctrl.4 ' Enable PLL Oscillator
'Bitwait Osc_status.4 , Set ' wait until the pll clock reference source is stable
'Clk_ctrl = &B0000_0100 ' switch system clock to pll
'Config Sysclock = Pll , Prescalea = 1 , Prescalebc = 1_1
'-----PWM-----
$lib "xmega.lib" : $external _xmegafix_clear : $external _xmegafix_rol_r1014
'Config Priority = Static , Vector = Application , Lo = Enabled 'Enable Lo Level Interrupts
Config Porte.0 = Output
Config Tce0 = Pwm , Prescale = 1 , Comparea = Enabled
'SET Resolution of PWM (min. = &H0003 ..... max. = &HFFFF)
'Tce0_per = &H0320 'Set Period = H0320=800 >>> 32M/800=40KHz
'Tce0_cca = 80 'duty cycle = Tce0_cca/800
Tce0_per = &H00A0 'Set Period = H00A0=160 >>> 32M/160=200KHz
Tce0_cca = 50 'duty cycle = Tce0_cca/160

'Tce0_per = &H0140
'Tce0_cca = 10 'duty cycle = Tce0_cca/320

'----- Pin Config -----
'Config Porte.4 = Output 'LCD Backlight
'Lcdbacklight Alias Porte.4
Config Portr.0 = Output 'LED 0
Led0 Alias Portr.0
Config Portr.1 = Output 'LED 1
Led1 Alias Portr.1

'Config Pine.5 = Input
'Sw0 Alias Pine.5
Config Pinf.1 = Input
Sw1 Alias Pinf.1
Config Pinf.2 = Input
Sw2 Alias Pinf.2

'Config Portc.0 = Output ' J1_1
'Pulse_x_out Alias Portc.0
'Config Portc.1 = Output ' J1_2
'Direction_x Alias Portc.1

'Config Portc.2 = Output ' J1_3
'Pulse_y_out Alias Portc.2
'Config Portc.3 = Output ' J1_4
'Direction_y Alias Portc.3

```

'Config Portc.5 = Output
'Laser_Trigger Alias Portc.5

' J1_6

'Config Portc.6 = Output
'Enable_Stepper_X Alias Portc.6
'Config Portc.7 = Output
'Enable_Stepper_Y Alias Portc.7

' J1_7

' J1_8

'Config PortE.0 = Output
'Pulse_x_out Alias PortE.0

Config PortD.0 = Output
Pulse_x_out Alias PortD.0

Config PortE.1 = Output
Direction_x Alias PortE.1

Config PortE.2 = Output
Pulse_y_out Alias PortE.2
Config PortE.3 = Output
Direction_y Alias PortE.3
Config PortD.3 = Output
Laser_Trigger Alias PortD.3

Config PortD.2 = Output
Enable_Stepper_X Alias PortD.2
Config PortD.1 = Output
Enable_Stepper_Y Alias PortD.1

Config Pine.5 = Input
Sw_Enter Alias Pine.5

'Config Pinf.1 = Input
'Sw_Right Alias Pinf.1
Config PinB.1 = Input
Sw_Right Alias PinB.1
Config PinB.0 = Input
Sw_Left Alias PinB.0

'Config Pinf.2 = Input
'Sw_Up Alias Pinf.2
Config PinB.2 = Input
Sw_Up Alias PinB.2
Config PinA.4 = Input
Sw_Down Alias PinA.4

```

'----- Timer -----
Config Tcc0 = Normal , Prescale = 1

'----- Sub Declare -----

Declare Sub Pulse_x
Declare Sub Pulse_y
Declare Sub Pulse_Laser

Declare Sub PulsePerPoint (byval NPulse As Integer)

Declare sub draw_Square_1mm
Declare sub Square_1mm_Shift_Up
Declare sub Square_1mm_Shift_Down
Declare sub Square_1mm_Shift_Left
Declare sub Square_1mm_Shift_Right
Declare sub draw_Alphabet_T
Declare sub draw_Alphabet_E
Declare sub draw_Alphabet_X
Declare sub draw_Alphabet_A
Declare sub draw_Alphabet_S
Declare Sub Enable_X
Declare Sub Disable_X
Declare Sub Enable_Y
Declare Sub Disable_Y
declare sub Stage_Initiate
declare sub X_Backlash_LR
declare sub X_Backlash_RL
declare sub Y_Backlash_UD
declare sub Y_Backlash_DU

'----- ADC -----
Config Adcb = Single , Convmode = Unsigned , Resolution = 12bit , Dma = Off , Reference = Int1v ,
Event_mode = None , Prescaler = 32 , Ch0_gain = 1 , Ch0_inp = Single_ended , Mux0 = 0

'----- LCD -----

'$lib "glcdeadogm128x6.lbx"
'Config Graphlcd = 128 * 64eadogm , A0 = Portd.0 , Sclk = Portd.1 , Si = Portd.3 , Cs1 = Portf.3 , Rst =
Porta.3

waitms 10
$lib "glcdeadogm128x6.lib"
Config Graphlcd = 128 * 64eadogm , A0 = Portc.2 , Sclk = Portc.0 , Si = Portc.1 , Cs1 = Portc.4 , Rst =
Portc.3      'large spi lcd
'Config Graphlcd = 128 * 64eadogm , A0 = PortE.2 , Sclk = PortE.0 , Si = PortE.1 , Cs1 = PortD.0 , Rst
= PortE.3      'large spi lcd

Glcddcmd &HAE          ' lcd off
Glcddcmd &HAF          ' lcd on
'Const Eadogm_rotate = 1      ' Rotate the LCD

```

```
'Glcdcmd &H22          'contrast set: 20 HEX-27 HEX
Glcdcmd &H26
'Glcdcmd &HA7          ' inverting the color
waitms 10
```

```
'----- Internal EEPROM -----
Config Eeprom = Mapped
```

```
'----- Variables -----
```

```
Dim I As long , J As long , k as long, A1 As long , A2 As long
dim x as long,y as long
Dim Lcdwave(128) As Integer          ' from 1 to 23
Dim Lcdpage As Integer , Lcddat As Integer
Dim W1 As Word , W2 As Word
```

```
Dim Duty As Integer
```

```
dim ii as long,jj as long
```

```
Dim PPP as Eram integer , Mod_Number as Eram integer , X_Step as Eram integer, Y_Step as Eram
integer, X_Points as Eram integer, Y_Points as Eram integer
Dim PPP_Buffer as integer , Mod_Number_Buffer as integer , X_Step_Buffer as integer,
Y_Step_Buffer as integer, X_Points_Buffer as integer, Y_Points_Buffer as integer
Dim X_Total_Pulse as Long , Y_Total_Pulse as Long
Dim Parameter_Counter as byte
```

```
Dim X0 as integer , Y0 as integer
```

```
'-----
```

```
'Do
' Set Pulse_x_out
' Set Direction_x
' Set Enable_Stepper_x
' wait 1
' Reset Pulse_x_out
' Reset Direction_x
' Reset Enable_Stepper_x
' wait 1
'Loop
```

```

'Set Lcdbacklight
set Led0
set Led1
set Enable_Stepper_X
set Enable_Stepper_Y

reset Laser_Trigger

'Glcdcmd &HAE           ' lcd off
'Glcdcmd &HAF           ' lcd on
"Const Eadogm_rotate = 1   ' Rotate the LCD
'Glcdcmd &H22           'contrast set: 20 HEX-27 HEX
'Glcdcmd &HA7           ' inverting the color

'Cls
SetFont Font8x8tt

'Showpic 260 , 1 , Clearscreen
CLS

Lcdat 1 , 5 , "Stage Controller"
Wait 1
CLS

'.....
' Mod_Number =0 : Solid Square
' Variables: X_Step, Y_Step, X_Max, Y_Max, PPP

'Showpic 260 , 1 , Clearscreen

Goto MainLoop

Mod_Number = 1
X_Step= 250
y_Step= 250
X_Points = 100
Y_Points = 10
ppp = 1

MainLoop:
If Mod_Number = 1 then
  X_Step_Buffer = X_Step
  Y_Step_Buffer = Y_Step
  X_Points_Buffer = X_Points
  Y_Points_Buffer = Y_Points
  PPP_Buffer = PPP
  Lcdat 1 , 5 , "Prog:Solid Square"
  Lcdat 2 , 5 , "          "
  Lcdat 3 , 5 , "          "
  Lcdat 4 , 5 , "          "
  Lcdat 3 , 5 , "Xs="
  Lcdat 3 , 25 ,X_Step_Buffer
  Lcdat 3 , 65 , "Ys="
  Lcdat 3 , 90 , Y_Step_Buffer

```

```

Lcdat 2 , 5 , "Xp="
Lcdat 2 , 25 ,X_Points_Buffer
Lcdat 2 , 65 , "Yp="
Lcdat 2 , 90 , Y_Points_Buffer
Lcdat 4 , 5 , "PPP="
Lcdat 4 , 35 ,PPP_Buffer
If Sw_Right = 0 Then
  Waitms 300
  Parameter_Counter=1
  Do
    Lcdat 2 , 5 , "          "
    Lcdat 3 , 5 , "          "
    Lcdat 4 , 5 , "          "
    Lcdat 3 , 5 , "Xs="
    Lcdat 3 , 25 ,X_Step_Buffer
    Lcdat 3 , 65 , "Ys="
    Lcdat 3 , 90 , Y_Step_Buffer
    Lcdat 2 , 5 , "Xp="
    Lcdat 2 , 25 ,X_Points_Buffer
    Lcdat 2 , 65 , "Yp="
    Lcdat 2 , 90 , Y_Points_Buffer
    Lcdat 4 , 5 , "PPP="
    Lcdat 4 , 35 ,PPP_Buffer
    Select Case Parameter_Counter
      Case 1
        Lcdat 1 , 5 , " Xp Adjustment  "
        If Sw_Up = 0 Then X_Points_Buffer = X_Points_Buffer +1
        If Sw_Down = 0 Then X_Points_Buffer = X_Points_Buffer -1
      Case 2
        Lcdat 1 , 5 , " Yp Adjustment  "
        If Sw_Up = 0 Then Y_Points_Buffer = Y_Points_Buffer +1
        If Sw_Down = 0 Then Y_Points_Buffer = Y_Points_Buffer -1
      Case 3
        Lcdat 1 , 5 , " Xs Adjustment  "
        If Sw_Up = 0 Then X_Step_Buffer = X_Step_Buffer +1
        If Sw_Down = 0 Then X_Step_Buffer = X_Step_Buffer -1
      Case 4
        Lcdat 1 , 5 , " Ys Adjustment  "
        If Sw_Up = 0 Then Y_Step_Buffer = Y_Step_Buffer +1
        If Sw_Down = 0 Then Y_Step_Buffer = Y_Step_Buffer -1
      Case 5
        Lcdat 1 , 5 , " PPP Adjustment  "
        If Sw_Up = 0 Then PPP_Buffer = PPP_Buffer +1
        If Sw_Down = 0 Then PPP_Buffer = PPP_Buffer -1
    End Select
  End If
  If Sw_Right = 0 Then
    waitms 300
    Parameter_Counter = Parameter_Counter +1
    if Parameter_Counter > 5 then Parameter_Counter =1
  End If
  If Sw_Left = 0 Then
    Wait 1
    goto MainLoop
  End If
  If Sw_Enter = 0 Then
    Lcdat 1 , 5 , " Saving...  "
    X_Step=X_Step_Buffer
    Y_Step=Y_Step_Buffer
    X_Points=X_Points_Buffer

```

```

    Y_Points=Y_Points_Buffer
    PPP=PPP_Buffer
    Wait 1
    goto MainLoop
End If
Waitms 100
Loop
End If
If Sw_Enter = 0 Then
    Lcdat 1 , 5 , "Ready To Start?  "
    Wait 1
    Do
        If Sw_Enter = 0 Then
            Lcdat 1 , 5 , "Starting the Program"
            goto Start_P1
        End If
        If SW_Left = 0 then
            Lcdat 1 , 5 , "Cancel Program Start"
            Wait 1
            goto MainLoop
        End if
    Loop
Start_P1:
    Lcdat 1 , 5 , "          "
    reset led1
    set led0
    Enable_X
    Enable_Y
    Stage_Initiate
    for y=1 to Y_Points_Buffer step 1
        X_Backlash_LR
        for x=1 to X_Points_Buffer step 1
            Lcdat 1 , 5 , "          "
            Lcdat 1 , 5 , "X="
            Lcdat 1 , 20 , x
            Lcdat 1 , 65 , "Y="
            Lcdat 1 , 85 , y
            For i = 1 To PPP_Buffer Step 1
                Pulse_Laser
            Next i
            Direction_x = 0
            For l = 1 To X_Step_Buffer*5 Step 1      ' 5 pulses = 1 microm
                Pulse_x
            Next l
        next x
        Direction_y = 1
        For l = 1 To Y_Step_Buffer*5 Step 1      ' 5 pulses = 1 microm
            Pulse_y
        Next l
        X_Total_Pulse = X_Points_Buffer * X_Step_Buffer
        X_Total_Pulse = X_Total_Pulse *5
        Y_Total_Pulse = Y_Points_Buffer * Y_Step_Buffer
        Y_Total_Pulse = Y_Total_Pulse *5
        ' Return x to home position
        Direction_x = 1
        For l = 1 To X_Total_Pulse Step 1      '
            Pulse_x
        Next l
    next y

```

```

set led1
' to return y back to home position
Direction_y = 0
For I = 1 To Y_Total_Pulse Step 1
    Pulse_y
Next I
Disable_X
Disable_Y
set led1
Cls
Lcdat 1 , 5 , "X=1"
Lcdat 2 , 5 , "Y=1"
End if
End If
If Mod_Number = 2 then
Lcdat 1 , 5 , " Manual Adjustment"
Lcdat 2 , 5 , "          "
Lcdat 3 , 5 , "          "
Lcdat 4 , 5 , "          "

If Sw_Enter = 0 Then
Waitms 300
X0=0
Y0=0
Enable_X
Enable_Y
Do
Lcdat 2 , 5 , "          "
Lcdat 3 , 5 , "          "
Lcdat 4 , 5 , "          "
Lcdat 3 , 5 , "X0="
Lcdat 3 , 25 ,X0
Lcdat 3 , 65 , "Y0="
Lcdat 3 , 90 , Y0
Lcdat 2 , 5 , "Xp="
Lcdat 2 , 25 ,X_Points_Buffer
Lcdat 2 , 65 , "Yp="
Lcdat 2 , 90 , Y_Points_Buffer
Lcdat 4 , 5 , "PPP="
Lcdat 4 , 35 ,PPP_Buffer
If Sw_Left = 0 Then
X0=X0-50
Direction_x = 0
For I = 1 To 250 Step 1
    Pulse_x
Next I
Waitms 300
End If
If Sw_Right = 0 Then
X0=X0+50
Direction_x = 1
For I = 1 To 250 Step 1
    Pulse_x
Next I
Waitms 300
End If
If Sw_Down = 0 Then
Y0=Y0-50

```

```

    Direction_y = 1
    For I = 1 To 250 Step 1      ' 5 pulses = 1 microm
        Pulse_y
    Next I
    Waitms 300
End If
If Sw_Up = 0 Then
    Y0=Y0+50
    Direction_y = 0
    For I = 1 To 250 Step 1      ' 5 pulses = 1 microm
        Pulse_y
    Next I
    Waitms 300
End If
If Sw_Enter = 0 Then
    Waitms 300
    Disable_X
    Disable_Y
    Goto MainLoop
End If
Loop

End If

```

```

End If
If Mod_Number = 3 then
    Lcdat 1 , 5 , "  Program 3      "
    Lcdat 2 , 5 , "                "
    Lcdat 3 , 5 , "                "
    Lcdat 4 , 5 , "                "
End If
Mod_Number_Buffer = Mod_Number
if Sw_Up = 0 then
    Mod_Number_Buffer = Mod_Number_Buffer +1
    Mod_Number = Mod_Number_Buffer
    waitms 300
end if
if Sw_Down = 0 then
    Mod_Number_Buffer = Mod_Number_Buffer - 1
    Mod_Number = Mod_Number_Buffer
    waitms 300
end if
If Mod_Number_Buffer < 1 then
    Mod_Number_Buffer =3          ' Max numbers of programs
    Mod_Number = Mod_Number_Buffer
End If
If Mod_Number_Buffer > 3 then      ' Max numbers of programs
    Mod_Number_Buffer =1
    Mod_Number = Mod_Number_Buffer
End IF
waitms 100
Goto MainLoop

```

```

End

$include "font8x8TT.font"
$include "my12_16.font"
Clearscreen:
$bgf "Clearscreen.bgf"

Sub Pulse_x
  Tcc0_per = 500 '200
  Tcc0_intflags.0 = 1
  Set Pulse_x_out
  Bitwait Tcc0_intflags.0 , Set
  Tcc0_per = 500 '200
  Tcc0_intflags.0 = 1
  Reset Pulse_x_out
  Bitwait Tcc0_intflags.0 , Set
End Sub

Sub Pulse_y
  Tcc0_per = 500 '200
  Tcc0_intflags.0 = 1
  Set Pulse_y_out
  Bitwait Tcc0_intflags.0 , Set
  Tcc0_per = 500 '200
  Tcc0_intflags.0 = 1
  Reset Pulse_y_out
  Bitwait Tcc0_intflags.0 , Set
End Sub

Sub Pulse_Laser
  set Laser_Trigger
  waitus 20
  reset Laser_Trigger
  waitms 100
End Sub

Sub PulsePerPoint (byval NPulse as Integer)
  Local ii1 as integer
  For ii1 = 1 To NPulse Step 1
    Pulse_Laser
  Next ii1
End Sub

sub Enable_X
  reset Enable_Stepper_X
  waitms 100
End Sub
sub Disable_X
  set Enable_Stepper_X
  waitms 100
End Sub
sub Enable_Y
  reset Enable_Stepper_Y
  waitms 100
End Sub
sub Disable_Y
  set Enable_Stepper_Y
  waitms 100
End Sub

```

```

sub draw_Square_1mm
  Direction_x = 1
  for ii=1 to 20 step 1
    Pulse_Laser
    Pulse_Laser
    For jj = 1 To 250 Step 1      '50um
      Pulse_x
    Next jj
  next ii
  Direction_y = 1
  for ii=1 to 20 step 1
    Pulse_Laser
    Pulse_Laser
    For jj = 1 To 250 Step 1      '50um
      Pulse_y
    Next jj
  next ii
  Direction_x = 0
  for ii=1 to 20 step 1
    Pulse_Laser
    Pulse_Laser
    For jj = 1 To 250 Step 1      '50um
      Pulse_x
    Next jj
  next ii
  Direction_y = 0
  for ii=1 to 20 step 1
    Pulse_Laser
    Pulse_Laser
    For jj = 1 To 250 Step 1      '50um
      Pulse_y
    Next jj
  next ii
  Pulse_Laser
  Pulse_Laser
end sub

sub Square_1mm_Shift_Up
  Direction_y = 0
  For ii = 1 To 5000 Step 1      'for 1mm
    Pulse_y
  Next ii
end sub

sub Square_1mm_Shift_Down
  Direction_y = 1
  For ii = 1 To 5000 Step 1      'for 1mm
    Pulse_y
  Next ii
end sub

sub Square_1mm_Shift_Right
  Direction_x = 0
  For ii = 1 To 5000 Step 1      'for 1mm
    Pulse_x
  Next ii
end sub

sub Square_1mm_Shift_Left
  Direction_x = 1
  For ii = 1 To 5000 Step 1      'for 1mm

```



```
Square_1mm_Shift_Left
Square_1mm_Shift_Up
Square_1mm_Shift_Up
Square_1mm_Shift_Up
draw_Square_1mm
Square_1mm_Shift_Right
draw_Square_1mm
Square_1mm_Shift_Right
draw_Square_1mm
Square_1mm_Shift_Left
Square_1mm_Shift_Left
Square_1mm_Shift_Up
Square_1mm_Shift_Up
Square_1mm_Shift_Up
draw_Square_1mm
Square_1mm_Shift_Right
draw_Square_1mm
Square_1mm_Shift_Right
draw_Square_1mm
Square_1mm_Shift_Right
draw_Square_1mm
Square_1mm_Shift_Right
draw_Square_1mm
Square_1mm_Shift_Right
Square_1mm_Shift_Right
end sub
```

```
sub draw_Alphabet_X
draw_Square_1mm
Square_1mm_Shift_Down
draw_Square_1mm
Square_1mm_Shift_Down
Square_1mm_Shift_Right
draw_Square_1mm
Square_1mm_Shift_Down
Square_1mm_Shift_Right
draw_Square_1mm
Square_1mm_Shift_Down
Square_1mm_Shift_Right
draw_Square_1mm
Square_1mm_Shift_Down
Square_1mm_Shift_Right
draw_Square_1mm
Square_1mm_Shift_Left
Square_1mm_Shift_Left
Square_1mm_Shift_Left
Square_1mm_Shift_Left
draw_Square_1mm
Square_1mm_Shift_Up
draw_Square_1mm
Square_1mm_Shift_Right
Square_1mm_Shift_Up
draw_Square_1mm
Square_1mm_Shift_Right
Square_1mm_Shift_Up
Square_1mm_Shift_Right
Square_1mm_Shift_Up
draw_Square_1mm
```

```
Square_1mm_Shift_Right  
Square_1mm_Shift_Up  
draw_Square_1mm
```

```
Square_1mm_Shift_Up  
draw_Square_1mm  
Square_1mm_Shift_Right  
Square_1mm_Shift_Right  
end sub
```

```
sub draw_Alphabet_A  
Square_1mm_Shift_Right  
draw_Square_1mm  
Square_1mm_Shift_Right  
draw_Square_1mm  
Square_1mm_Shift_Right  
draw_Square_1mm  
Square_1mm_Shift_Right  
Square_1mm_Shift_Down  
draw_Square_1mm  
Square_1mm_Shift_Down  
draw_Square_1mm  
Square_1mm_Shift_Down  
draw_Square_1mm  
Square_1mm_Shift_Down  
draw_Square_1mm  
Square_1mm_Shift_Down  
draw_Square_1mm  
Square_1mm_Shift_Left  
Square_1mm_Shift_Left  
Square_1mm_Shift_Left  
Square_1mm_Shift_Left  
draw_Square_1mm  
Square_1mm_Shift_UP  
draw_Square_1mm  
Square_1mm_Shift_UP  
draw_Square_1mm  
Square_1mm_Shift_UP  
draw_Square_1mm  
Square_1mm_Shift_UP  
draw_Square_1mm  
Square_1mm_Shift_UP  
draw_Square_1mm  
Square_1mm_Shift_Down  
Square_1mm_Shift_Down  
Square_1mm_Shift_Down  
Square_1mm_Shift_Right  
draw_Square_1mm  
Square_1mm_Shift_Right  
draw_Square_1mm  
Square_1mm_Shift_Right  
draw_Square_1mm  
Square_1mm_Shift_Right  
Square_1mm_Shift_UP  
Square_1mm_Shift_UP  
Square_1mm_Shift_UP  
Square_1mm_Shift_UP
```

```
Square_1mm_Shift_Right  
Square_1mm_Shift_Right  
end sub
```

```
sub draw_Alphabet_S  
Square_1mm_Shift_Down  
draw_Square_1mm  
Square_1mm_Shift_Down  
draw_Square_1mm  
Square_1mm_Shift_Down  
Square_1mm_Shift_Right  
draw_Square_1mm  
Square_1mm_Shift_Right  
draw_Square_1mm  
Square_1mm_Shift_Right  
draw_Square_1mm  
Square_1mm_Shift_Down  
draw_Square_1mm  
Square_1mm_Shift_Down  
draw_Square_1mm  
Square_1mm_Shift_Down  
Square_1mm_Shift_Left  
draw_Square_1mm  
Square_1mm_Shift_Left  
draw_Square_1mm  
Square_1mm_Shift_Left  
draw_Square_1mm  
Square_1mm_Shift_Left  
draw_Square_1mm  
Square_1mm_Shift_Left  
draw_Square_1mm  
Square_1mm_Shift_UP  
Square_1mm_Shift_UP  
Square_1mm_Shift_UP  
Square_1mm_Shift_UP  
Square_1mm_Shift_UP  
Square_1mm_Shift_UP  
Square_1mm_Shift_Right  
draw_Square_1mm  
Square_1mm_Shift_Right  
draw_Square_1mm  
Square_1mm_Shift_Right  
draw_Square_1mm  
Square_1mm_Shift_Right  
draw_Square_1mm  
Square_1mm_Shift_Right  
draw_Square_1mm  
Square_1mm_Shift_Right  
Square_1mm_Shift_Right  
end sub
```

```
sub Stage_Initiate  
Square_1mm_Shift_Left  
Square_1mm_Shift_Left  
Square_1mm_Shift_Left  
Square_1mm_Shift_Left  
Square_1mm_Shift_Right  
Square_1mm_Shift_Right  
Square_1mm_Shift_Right  
Square_1mm_Shift_Right  
Square_1mm_Shift_Up  
Square_1mm_Shift_Up  
Square_1mm_Shift_Up  
end sub
```

```

Square_1mm_Shift_Up
Square_1mm_Shift_Down
Square_1mm_Shift_Down
Square_1mm_Shift_Down
Square_1mm_Shift_Down
Square_1mm_Shift_Left
Square_1mm_Shift_Left
Square_1mm_Shift_Left
Square_1mm_Shift_Left
Square_1mm_Shift_Right
Square_1mm_Shift_Right
Square_1mm_Shift_Right
Square_1mm_Shift_Right
Square_1mm_Shift_Up
Square_1mm_Shift_Up
Square_1mm_Shift_Up
Square_1mm_Shift_Up
Square_1mm_Shift_Down
Square_1mm_Shift_Down
Square_1mm_Shift_Down
Square_1mm_Shift_Down
end sub
sub X_Backlash_LR
  Square_1mm_Shift_Left
  Square_1mm_Shift_Left
  Square_1mm_Shift_Right
  Square_1mm_Shift_Right
end sub
sub X_Backlash_RL
  Square_1mm_Shift_Right
  Square_1mm_Shift_Right
  Square_1mm_Shift_Left
  Square_1mm_Shift_Left
end sub
sub Y_Backlash_UD
  Square_1mm_Shift_UP
  Square_1mm_Shift_UP
  Square_1mm_Shift_Down
  Square_1mm_Shift_Down
end sub
sub Y_Backlash_DU
  Square_1mm_Shift_Down
  Square_1mm_Shift_Down
  Square_1mm_Shift_UP
  Square_1mm_Shift_UP
end sub

```

REFERENCES

- [1] D. Malamud and L. A. Tabak, *Saliva as a diagnostic fluid* (Annals of the New York Academy of Sciences,, no. 694). New York, N.Y.: New York Academy of Sciences, 1993, pp. xii, 348 p.
- [2] C. M. Plotz and J. M. Singer, "The latex fixation test. I. Application to the serologic diagnosis of rheumatoid arthritis," *Am J Med*, vol. 21, no. 6, pp. 888-92, Dec 1956.
- [3] R. C. Wong and H. Y. Tse, *Lateral flow immunoassay*. New York, NY: Springer, 2009, pp. xii, 223 p.
- [4] B. Kavosi, R. Hallaj, H. Teymourian, and A. Salimi, "Au nanoparticles/PAMAM dendrimer functionalized wired ethyleneamine-viologen as highly efficient interface for ultra-sensitive alpha-fetoprotein electrochemical immunosensor," *Biosens Bioelectron*, vol. 59, pp. 389-96, Sep 15 2014.
- [5] B. S. Delmulle, S. M. De Saeger, L. Sibanda, I. Barna-Vetro, and C. H. Van Peteghem, "Development of an immunoassay-based lateral flow dipstick for the rapid detection of aflatoxin B1 in pig feed," *J Agric Food Chem*, vol. 53, no. 9, pp. 3364-8, May 4 2005.
- [6] J. Wu and M. Gu, "Microfluidic sensing: state of the art fabrication and detection techniques," *J Biomed Opt*, vol. 16, no. 8, p. 080901, Aug 2011.
- [7] R. Mukhopadhyay, "When PDMS isn't the best. What are its weaknesses, and which other polymers can researchers add to their toolboxes?," *Anal Chem*, vol. 79, no. 9, pp. 3248-53, May 1 2007.
- [8] J. C. McDonald *et al.*, "Fabrication of microfluidic systems in poly(dimethylsiloxane)," *Electrophoresis*, vol. 21, no. 1, pp. 27-40, Jan 2000.

- [9] U. M. Attia, S. Marson, and J. R. Alcock, "Micro-injection moulding of polymer microfluidic devices," (in English), *Microfluidics and Nanofluidics*, vol. 7, no. 1, pp. 1-28, Jul 2009.
- [10] H. Cao, J. O. Tegenfeldt, R. H. Austin, and S. Y. Chou, "Gradient nanostructures for interfacing microfluidics and nanofluidics," (in English), *Applied Physics Letters*, vol. 81, no. 16, pp. 3058-3060, Oct 14 2002.
- [11] J. Rossier, F. Reymond, and P. E. Michel, "Polymer microfluidic chips for electrochemical and biochemical analyses," *Electrophoresis*, vol. 23, no. 6, pp. 858-67, Mar 2002.
- [12] T. Mappes, S. Achenbach, and J. Mohr, "X-ray lithography for devices with high aspect ratio polymer submicron structures," (in English), *Microelectronic Engineering*, vol. 84, no. 5-8, pp. 1235-1239, May-Aug 2007.
- [13] A. W. Martinez, S. T. Phillips, G. M. Whitesides, and E. Carrilho, "Diagnostics for the Developing World: Microfluidic Paper-Based Analytical Devices," (in English), *Analytical Chemistry*, vol. 82, no. 1, pp. 3-10, Jan 1 2010.
- [14] M. B. Esch, S. Kapur, G. Irizarry, and V. Genova, "Influence of master fabrication techniques on the characteristics of embossed microfluidic channels," *Lab Chip*, vol. 3, no. 2, pp. 121-7, May 2003.
- [15] S. J. Ahn, D. W. Kim, H. S. Kim, K. H. Cho, and S. S. Choi, "Laser fabrication of micron-size apertures for electron beam microcolumns," (in English), *Applied Physics a-Materials Science & Processing*, vol. 69, pp. S527-S530, Dec 1999.
- [16] D. K. Campbell and D. W. Sweeney, "Materials processing with CO₂ laser holographic scanner systems," *Appl Opt*, vol. 17, no. 23, pp. 3727-37, Dec 1 1978.

- [17] C. Rehbock *et al.*, "Current state of laser synthesis of metal and alloy nanoparticles as ligand-free reference materials for nano-toxicological assays," (in English), *Beilstein Journal of Nanotechnology*, vol. 5, pp. 1523-1541, Sep 12 2014.
- [18] B. Jaeggi, B. Neuenschwander, M. Schmid, M. Murali, J. Zuercher, and U. Hunziker, "Influence of the Pulse Duration in the ps-Regime on the Ablation Efficiency of Metals," (in English), *Lasers in Manufacturing 2011: Proceedings of the Sixth International Wlt Conference on Lasers in Manufacturing, Vol 12, Pt B*, vol. 12, pp. 164-171, 2011.
- [19] A. H. Hamad, K. S. Khashan, and A. A. Hadi, "Laser Ablation in Different Environments and Generation of Nanoparticles," (in English), *Applications of Laser Ablation - Thin Film Deposition, Nanomaterial Synthesis and Surface Modification*, pp. 177-196, 2016.
- [20] C. Momma *et al.*, "Short-pulse laser ablation of solid targets," (in English), *Optics Communications*, vol. 129, no. 1-2, pp. 134-142, Aug 1 1996.
- [21] J. Chai, F. Lu, B. Li, and D. Y. Kwok, "Wettability interpretation of oxygen plasma modified poly(methyl methacrylate)," *Langmuir*, vol. 20, no. 25, pp. 10919-27, Dec 7 2004.
- [22] C. Situma, A. J. Moehring, M. A. F. Noor, and S. A. Soper, "Immobilized molecular beacons: A new strategy using UV-activated poly(methyl methacrylate) surfaces to provide large fluorescence sensitivities for reporting on molecular association events," (in English), *Analytical Biochemistry*, vol. 363, no. 1, pp. 35-45, Apr 1 2007.
- [23] Y. P. Jiao and F. Z. Cui, "Surface modification of polyester biomaterials for tissue engineering," *Biomed Mater*, vol. 2, no. 4, pp. R24-37, Dec 2007.

- [24] R. L. Williams, D. J. Wilson, and N. P. Rhodes, "Stability of plasma-treated silicone rubber and its influence on the interfacial aspects of blood compatibility," *Biomaterials*, vol. 25, no. 19, pp. 4659-73, Aug 2004.
- [25] S. L. Llopis, J. Osiri, and S. A. Soper, "Surface modification of poly(methyl methacrylate) microfluidic devices for high-resolution separations of single-stranded DNA," *Electrophoresis*, vol. 28, no. 6, pp. 984-93, Mar 2007.
- [26] T. Liang, H. Q. Li, X. J. Lai, X. J. Su, L. Zhang, and X. R. Zeng, "A facile approach to UV-curable super-hydrophilic polyacrylate coating film grafted on glass substrate," (in English), *Journal of Coatings Technology and Research*, vol. 13, no. 6, pp. 1115-1121, Nov 2016.
- [27] W. S. Choi and S. H. Ryu, "Enhancement of Dispersion of Carbon Nanotube and Physical Properties of Poly(styrene-co-acrylonitrile)/Multiwalled Carbon Nanotube Nanocomposite via Surface Initiated ATRP," (in English), *Journal of Applied Polymer Science*, vol. 116, no. 5, pp. 2930-2936, Jun 5 2010.
- [28] A. J. Keefe, N. D. Brault, and S. Y. Jiang, "Suppressing Surface Reconstruction of Superhydrophobic PDMS Using a Superhydrophilic Zwitterionic Polymer," (in English), *Biomacromolecules*, vol. 13, no. 5, pp. 1683-1687, May 2012.
- [29] T. Govindarajan and R. Shandas, "A Survey of Surface Modification Techniques for Next-Generation Shape Memory Polymer Stent Devices," (in English), *Polymers*, vol. 6, no. 9, pp. 2309-2331, Sep 2014.
- [30] A. I. Kontos, A. G. Kontos, D. S. Tsoukleris, G. D. Vlachos, and P. Falaras, "Superhydrophilicity and photocatalytic property of nanocrystalline titania sol-gel films," (in English), *Thin Solid Films*, vol. 515, no. 18, pp. 7370-7375, Jun 25 2007.

- [31] X. F. Zhou, X. F. Guo, W. P. Ding, and Y. Chen, "Superhydrophobic or superhydrophilic surfaces regulated by micro-nano structured ZnO powders," (in English), *Applied Surface Science*, vol. 255, no. 5, pp. 3371-3374, Dec 30 2008.
- [32] S. Ganjoo, R. Azimirad, O. Akhavan, and A. Z. Moshfegh, "Persistent superhydrophilicity of sol-gel derived nanoporous silica thin films," (in English), *Journal of Physics D-Applied Physics*, vol. 42, no. 2, Jan 21 2009.
- [33] A. Andrady, M. B. Amin, S. H. Hamid, X. Z. Hu, and A. Torikai, "Effects of Increased Solar Ultraviolet-Radiation on Materials," (in English), *Ambio*, vol. 24, no. 3, pp. 191-196, May 1995.
- [34] K. G. Marra, T. M. Chapman, and J. M. Orban, "Determination of low critical surface tensions of novel fluorinated poly(amide urethane) block copolymers .3. Siloxane-containing side chains," (in English), *Macromolecules*, vol. 29, no. 23, pp. 7553-7558, Nov 4 1996.
- [35] P.-G. de Gennes, F. o. Brochard-Wyart, and D. Quéré, *Capillarity and wetting phenomena : drops, bubbles, pearls, waves*. New York: Springer, 2004, pp. xv, 291 p.
- [36] F. M. Chang, Y. J. Sheng, H. Chen, and H. K. Tsao, "From superhydrophobic to superhydrophilic surfaces tuned by surfactant solutions," (in English), *Applied Physics Letters*, vol. 91, no. 9, Aug 27 2007.
- [37] Y. Kakizawa *et al.*, "Solution properties of double-tailed cationic surfactants having ferrocenyl groups in their hydrophobic moieties," (in English), *Langmuir*, vol. 12, no. 4, pp. 921-924, Feb 21 1996.

- [38] M. T. Khorasani, H. Mirzadeh, and Z. Kermani, "Wettability of porous polydimethylsiloxane surface: morphology study," (in English), *Applied Surface Science*, vol. 242, no. 3-4, pp. 339-345, Apr 15 2005.
- [39] G. D. Tsiibidis, E. Stratakis, and K. E. Aifantis, "Thermoplastic deformation of silicon surfaces induced by ultrashort pulsed lasers in submelting conditions (vol 111, 053502, 2012)," (in English), *Journal of Applied Physics*, vol. 112, no. 8, Oct 15 2012.
- [40] V. Zorba *et al.*, "Making silicon hydrophobic: wettability control by two-lengthscale simultaneous patterning with femtosecond laser irradiation," (in English), *Nanotechnology*, vol. 17, no. 13, pp. 3234-3238, Jul 14 2006.
- [41] A. Bensaoula, C. Boney, R. Pillai, G. A. Shafeev, A. V. Simakin, and D. Starikov, "Arrays of 3D micro-columns generated by laser ablation of Ta and steel: modelling of a black body emitter," (in English), *Applied Physics a-Materials Science & Processing*, vol. 79, no. 4-6, pp. 973-975, Sep 2004.
- [42] R. Younkin, J. E. Carey, E. Mazur, J. A. Levinson, and C. M. Friend, "Infrared absorption by conical silicon microstructures made in a variety of background gases using femtosecond-laser pulses," (in English), *Journal of Applied Physics*, vol. 93, no. 5, pp. 2626-2629, Mar 1 2003.
- [43] E. Carpenne, D. Hoche, and P. Schaaf, "Fundamentals of Laser-Material Interactions," (in English), *Laser Processing of Materials: Fundamentals, Applications and Developments*, vol. 139, pp. 21-47, 2010.
- [44] S. Ye, Q. Cao, Q. S. Wang, T. Y. Wang, and Q. Peng, "A highly efficient, stable, durable, and recyclable filter fabricated by femtosecond laser drilling of a titanium foil for oil-water separation," (in English), *Scientific Reports*, vol. 6, Nov 21 2016.

- [45] G. Chitnis, Z. W. Ding, C. L. Chang, C. A. Savran, and B. Ziaie, "Laser-treated hydrophobic paper: an inexpensive microfluidic platform," (in English), *Lab on a Chip*, vol. 11, no. 6, pp. 1161-1165, 2011.
- [46] R. N. Wenzel, "Resistance of solid surfaces to wetting by water," (in English), *Industrial and Engineering Chemistry*, vol. 28, pp. 988-994, 1936.
- [47] E. W. Washburn, "The dynamics of capillary flow.," (in English), *Physical Review*, vol. 17, no. 3, pp. 273-283, Mar 1921.
- [48] S. Cito, "Numerical and experimental study of flow and wall mass transfer rates in capillary driven flows in microfluidic channels," 2009.
- [49] H. R. Ai, X. Q. Li, S. Y. Shi, Y. Zhang, and T. Q. Liu, "Measurement of Wenzel roughness factor by laser scanning confocal microscopy," (in English), *Rsc Advances*, vol. 7, no. 12, pp. 7052-7059, 2017.
- [50] V. Kumar, C. K. Harris, A. Bronson, S. Shantha-Kumar, and A. Medina, "High-Temperature Liquid Metal Infusion Considering Surface Tension-Viscosity Dissipation," (in English), *Metallurgical and Materials Transactions B-Process Metallurgy and Materials Processing Science*, vol. 47, no. 1, pp. 108-115, Feb 2016.
- [51] C. H. Bosanquet, "On the flow of liquids into capillary tubes.," (in English), *Philosophical Magazine*, vol. 45, no. 267, pp. 525-531, Mar 1923.
- [52] D. Yang, M. Krasowska, C. Priest, M. N. Popescu, and J. Ralston, "Dynamics of Capillary-Driven Flow in Open Microchannels," (in English), *Journal of Physical Chemistry C*, vol. 115, no. 38, pp. 18761-18769, Sep 29 2011.

- [53] M. M. Cooper, L. C. Williams, and S. M. Underwood, "Student Understanding of Intermolecular Forces: A Multimodal Study," (in English), *Journal of Chemical Education*, vol. 92, no. 8, pp. 1288-1298, Aug 2015.
- [54] D. Kim and A. E. Herr, "Protein immobilization techniques for microfluidic assays," (in English), *Biomicrofluidics*, vol. 7, no. 4, Jul 2013.